MDM2 induces EMT via the B-Raf signaling pathway through 14-3-3

MENGTING OU[1], XICHAO XU[1], YING CHEN[1], LI LI[1], LU ZHANG[1], YI LIAO[2],
WEICHAO SUN[1], CHRISTINE QUACH[3], JIANGUO FENG[4] and LILING TANG[1]

[1]Key Laboratory of Biorheological Science and Technology, Ministry of Education, College of Bioengineering,
Chongqing University; [2]Department of Cardiothoracic Surgery, Southwest Hospital, Third Military Medical University,
Chongqing 400044, P.R. China; [3]Department ribosomal of Molecular Microbiology and Immunology, University of
Southern California, Los Angeles, CA 90033, USA; [4]Department of Anesthesiology, The Affiliated Hospital of
Southwest Medical University, Luzhou, Sichuan 646000, P.R. China

Abstract. MDM2 proto-oncogene, E3 ubiquitin protein ligase (MDM2) is a well-known oncogene and has been reported to be closely associated with epithelial-to-mesenchymal transition (EMT). The present study first demonstrated that the expression levels of MDM2 were markedly increased in TGF-β-induced EMT using quantitative PCR and western blotting. In addition, MDM2 was demonstrated to be associated with pathological grade in clinical glioma samples by immunohistochemical staining. Furthermore, overexpression of MDM2 promoted EMT in glioma, lung cancer and breast cancer cell lines using a scratch wound migration assay.

Correspondence to: Dr Liling Tang, Key Laboratory of Biorheological Science and Technology, Ministry of Education, College of Bioengineering, Chongqing University, 174 Shazhengjie, Shapingba, Chongqing 400044, P.R. China
E-mail: tangliling@cqu.edu.cn

Dr Jianguo Feng, Department of Anesthesiology, The Affiliated Hospital of Southwest Medical University, 25 Taiping Street, Jiangyang, Luzhou, Sichuan 646000, P.R. China
E-mail: fengjianguo@swmu.edu.cn

Abbreviations: MDM2, MDM2 proto-oncogene, E3 ubiquitin protein ligase; EMT, epithelial-to-mesenchymal transition; 14-3-3, tyrosine 3-monooxygenase activation protein ε; B-RAF, B-Raf proto-oncogene, serine/threonine kinase; RSK, 90 KDa ribosomal protein S6 kinase; β-arrestin1, subtype 1 of β-arrestin protein family; β-arrestin2, subtype 2 of β-arrestin protein family; Snail, Snail family transcriptional repressor 1; Slug, Snail family transcriptional repressor 2; ZEB1, zinc finger E-box binding homeobox 1; E-CAD, E-cadherin; N-CAD, N-cadherin; VIM, vimentin; GSEA, Gene Set Enrichment Analysis; SqRT-PCR, semi-quantitative reverse transcription PCR; qPCR, quantitative PCR; p70S6K, ribosomal protein S6 kinase; 4EBP1, eukaryotic translation initiation factor 4E binding protein 1

Subsequently, the present study explored the mechanism by which MDM2 promoted EMT and revealed that MDM2 induced EMT by upregulating EMT-related transcription factors via activation of the B-Raf signaling pathway through tyrosine 3-monooxygenase activation protein ε using RNA sequencing and western blotting. This mechanism depended on the p53 gene. Furthermore, *in vivo* experiments and the colony formation experiment demonstrated that MDM2 could promote tumor progression and induce EMT via the B-Raf signaling pathway. Since EMT contributes to increased drug resistance in tumor cells, the present study also explored the relationship between MDM2 and drug sensitivity using an MTT assay, and identified that MDM2 promoted cell insensitivity to silibinin treatment in an EMT-dependent manner. This finding is crucial for the development of cancer therapies and can also provide novel research avenues for future biological and clinical studies.

Introduction

MDM2 proto-oncogene, E3 ubiquitin protein ligase (MDM2) is a well-known oncogene that has been reported to be closely associated with different disease phenotypes (1). MDM2 is a specific target gene of p53 and is a unique ubiquitin-protein ligase associated with numerous cancer types (1). MDM2 can transfer from the nucleus to the cytoplasm and degrade various substrates, such as p53 (2). In addition, MDM2 and p53 can form a negative-feedback loop (2). The p53 gene enhances MDM2 protein expression, while MDM2 inhibits p53 through simultaneously ubiquitinating and degrading p53 (2,3). P53 is a cancer suppressor the function of which can be eliminated by MDM2 activity (2,3). Therefore, MDM2 is related to tumor formation, anti-apoptosis effects and drug resistance (4,5).

Epithelial-to-mesenchymal transition (EMT) is a dynamic and complex process. When EMT occurs, epithelial cells change their morphology, lose their polarity, and acquire the features and potential of mesenchymal cells (6). EMT is involved in embryonic development, wound healing, invasion and metastasis in tumor cells (6). Notably, EMT serves

a crucial role in tumor progression (6). According to previous studies, the expression levels of MDM2 are increased in TGF-β-induced EMT (2,3,7,8). Therefore, MDM2 is an important part of tumor cell invasion, metastasis and the EMT process. In certain invasive ductal breast carcinoma models, overexpression of MDM2 promotes the invasion and migration of tumor cells (7). A previous study reported that MDM2 can promote EMT by upregulating the expression of Snail family transcriptional repressor 1 (*Snail*) in breast cancer cells (4). A number of articles have reported the close relationship between MDM2 and EMT in other cancer cells (4-8). MDM2 induces the migration of tumor cells by inhibiting E-cadherin (E-CAD) expression (7,8). However, to the best of our knowledge, the mechanism by which MDM2 promotes EMT is still unknown.

The MAPK/ERK signaling pathway is a complex and highly conserved cellular signaling pathway widely used in eukaryotic cells, and it is important for the occurrence, development and malignant transformation of tumors (9). Raf/MEK/ERK is a classical and important pathway involved in tumor development, leading to abnormal proliferation, invasion, growth and distant metastasis of malignant tumors (10). Various *in vitro* experiments have demonstrated the important roles of Raf/MEK/ERK signaling in the development of cancer; however, there are still numerous unknowns regarding the involvement of this pathway with cancer (9-11). A number of studies have reported that Raf/MEK/ERK signaling can participate in EMT, while the mechanism by which Raf/MEK/ERK signaling is involved in and affects EMT is unclear (9-11). Therefore, with the continuous progress and updating of diagnosis and treatment technology, the specific regulatory mechanism for the Raf/MEK/ERK signaling pathway to block its induction of tumor biological behavior has become a focus of current cancer research (9-11).

Tyrosine 3-monooxygenase activation protein ε (14-3-3) proteins are a family of highly conserved small proteins (12). At present, 14-3-3 proteins are regarded as a major class of molecular chaperones, with >200 proteins having been demonstrated to be targeted by them, and the list is still expanding (12). A turning point in understanding the role of 14-3-3 proteins was the discovery that 14-3-3 proteins bind to specific phosphorylated motifs in protein targets in 1996 (13). The majority of target proteins contain 14-3-3-binding motif(s) with the following amino acid sequences: RSXpSXP (mode I) and RXY/FXpSXP (mode II) or -pS/pTX(1-2)-CO$_2$H (mode III) (where X is not Pro) (14-16). Upon interaction with a target, 14-3-3 proteins alter target protein modifications, activities and cellular localizations, and thus regulate five major cellular functions: Cell cycle regulation, apoptosis, signal transduction, metabolism and intracellular protein trafficking (17-23). Notably, previous studies have revealed that B-Raf contains at least two binding sites for 14-3-3, and 14-3-3 could combine with B-Raf to affect the activation of B-Raf (14-16). It is interesting to note that 14-3-3 can deactivate B-Raf directly by making it locate to the cytoplasm (24-27). Under basal conditions, B-Raf phosphorylation creates docking sites for 14-3-3 proteins, resulting in the sequestration of B-Raf in the cytoplasm as an off-state (28,29). 14-3-3 deficiency can directly lead to B-Raf reactivation (28,29).

EMT contributes to the resistance of cancer cells to chemotherapy agents. According to previous studies, numerous chemicals have been used in cancer treatments (7,8,30-32). However, they often have little or no effect on cells that have undergone EMT (30). EMT is also involved in the drug resistance of breast cancer cells, and these resistant cancer cells exhibit increased migration and invasion activities (31,32). In some human glioma cell models, EMT is necessary for tumor cells to acquire resistance to drugs (33,34). Furthermore, EMT has been reported to be associated with drug resistance and sensitivity to numerous chemotherapeutics in non-small-cell lung carcinoma, breast cancer and bladder cancer (35,36).

Based on previous studies and data, the present study attempted to reveal the mechanism of MDM2-mediated induction of EMT. In addition, the present study aimed to explore whether p53 is involved in MDM2-mediated EMT. Since EMT contributes to the drug resistance of tumor cells, the present study also tried to reveal the relationship between MDM2 and drug sensitivity.

Materials and methods

Plasmid vector construction. Plasmid construction was performed as described in our previous studies (37-39). pLenti-CMV-MDM2-green fluorescent protein (GFP)-puro was constructed based on a plenti-CMV-puro backbone. The present study first PCR-amplified the MDM2 sequence lacking a termination codon using the plasmid pcDNA3.1-MDM2 as a template using the following primer pair and the Prime Star DNA Polymerase kit (Takara Bio, Inc.): Forward, 5'-CGC GCCACCATGGTGAGGAGCAGGCAAAT-3' and reverse, 5'-ACGCGGGGAAATAAG-3'. The PCR conditions used were as follows: 94˚C for 5 min; 94˚C for 30 sec; 56˚C for 60 sec; 72˚C for 1 min; 72˚C for 10 min; 4˚C for 10 min; cycle number, 35. PCR fragments were purified on a 1.5% agarose gel with ethidium bromide using the E.Z.N.A.® DNA Kit (Omega Bio-Tek, Inc.). A purified GFP cDNA fragment that lacked an initiation codon was PCR-amplified using plenti-CMV-GFP as a template by the following primer pair and the Prime Star DNA Polymerase kit (Takara Bio, Inc.): Forward, 5'-CGTCAG ATCCGCTAGCGCTACCGGTCG-3' and reverse, 5'-GCT TACTTGTACAGCTCGTCCATGCCG-3'. The PCR conditions used were as follows: 94˚C for 5 min; 94˚C for 30 sec; 55˚C for 30 sec; 72˚C for 30 sec; 72˚C for 10 min; 4˚C for 10 min; cycle number, 32. PCR fragments were purified on a 1.5% agarose gel with ethidium bromide using the E.Z.N.A.® DNA Kit (Omega Bio-Tek, Inc.). Overlap PCR was used to connect the purified MDM2 and GFP fragments using the following primer pair and the Prime Star DNA Polymerase kit (Takara Bio, Inc.): Forward, 5'-CGCGCCACCATGGTG AGGAGCAGGCAAAT-3' and reverse, 5'-GCTTACTTGTAC AGCTCGTCCATGCCG-3'. The PCR conditions used were as follows: 94˚C for 5 min; 94˚C for 30 sec; 56˚C for 60 sec; 72˚C for 1.5 min; 72˚C for 10 min; 4˚C for 10 min; cycle number, 35. PCR fragments were purified on a 1.5% agarose gel with ethidium bromide using the E.Z.N.A.® DNA Kit (Omega Bio-Tek, Inc.). Subsequently, Kozak sequences were added to the purified MDM2-GFP fragment and restriction enzyme sites for *Bam*HI and *Sal*I were also inserted. The recombinant fragment and pLenti-CMV-puro were digested with *Bam*HI

and *Sal*I (Takara Bio, Inc.), respectively, and then T4 ligase (Takara Bio, Inc.), was used to form the recombinant plasmid pLenti-CMV-MDM2-GFP-puro plasmid (Fig. S1A and B). In the present study, fragments and plasmids were digested with Takara QuickCut enzymes (Takara Bio, Inc.) and fragments and vectors were ligated with T4 ligase (Takara Bio, Inc.). In the present study, the pLenti-CMV-MDM2-GFP-puro plasmid sequencing process was conducted at Sangon Biotech Co., Ltd. *Stbl3* competent cells were used for plasmid transformation, and plasmid was extracted from *Stbl3* using a TIANGEN Kit. The pLenti-CMV-MDM2-GFP-puro plasmid sequencing result and original sequence were aligned using APE software (version 2.0; https://jorgensen.biology.utah.edu/wayned/ape/; Fig. S1B). Flag-14-3-3 and pcDNA3.1-p53 were purchased from Addgene, Inc.

Cell culture. U251MG, A549, MCF-7 and 293T cells (The Cell Bank of Type Culture Collection of The Chinese Academy of Sciences) were used in the present study. All cell lines were cultured at 37˚C with 5% CO_2. Ham's F-12K (Kaighn's) Medium (Thermo Fisher Scientific, Inc.) was used to culture A549 cells. U251MG, 293T and MCF-7 cells were cultured in DMEM with high glucose (HyClone; Cytiva). All media were supplemented with 10% FBS (Shanghai ExCell Biology, Inc.) and 100 μg/ml penicillin and streptomycin to make complete medium. Media were changed every other day. The inhibitors and activators used in the present study included an ERK inhibitor (FR180204; 10 μM, 24 h; cat. no. S7524; Selleck Chemicals), a 90 KDa ribosomal protein S6 kinase (RSK) inhibitor (SL0101; 50 μM, 24 h; cat. no. 77307-50-7; Sigma-Aldrich; Merck KGaA), vemurafenib (2 μM, 24 h; cat. no. A3004; APeXBIO Technology LLC), a MEK inhibitor U0126 (2 μM, 24 h; cat. no. 9903; Cell Signaling Technology, Inc.), TGF-β (10 ng/ml, 48 h; cat. no. 8915; Cell Signaling Technology, Inc.) and 20 mM Citrate pH 3.0 (Sterile) (cat. no. 9871; Cell Signaling Technology, Inc.). To examine TGF-β inducing EMT, U251 cells were incubated with 10 ng/ml TGF-β, and the control group was incubated with an equal volume of 20 mM citrate solution buffer, which was the buffer solution for TGF-β.

Plasmid transfection. pcDNA6B, pcDNA6B-Flag-14-3-3, pcDNA3.1 and pcDNA3.1-p53 were purchased from Addgene, Inc. Before transfection, MDM2-GFP stable cells were digested by tryptase that contained EDTA when the cells were 80% confluent. Then, $2x10^5$ cells/well were seeded into six-well plates (Suzhou Beaver Biomedical Engineering Co., Ltd.). pcDNA6B-Flag-14-3-3 or pcDNA3.1-p53 plasmid (2 μg) were transfected using PloyFect Effectene Transfection Reagent (Qiagen, Inc.) according to the manufacturer's protocols when cells were 60-80% confluent. Related empty vector (2 μg) was also transfected into MDM2-GFP stable cells using PloyFect as a control group. Cells were cultured at 37˚C with 5% CO_2 for 8 h, and then the media were replaced with fresh media. After transfection, cells were cultured at 37˚C with 5% CO_2 for 36 h. When the transfection was finished, cells were harvested in 1.5-ml microcentrifuge tubes for determination of gene overexpression by quantitative PCR (qPCR). Samples successfully transfected with plasmids were further tested by western blotting.

Co-transfection and lentivirus transduction. According to the manufacturer's protocols of the PloyFect Effectene Transfection Reagent (Qiagen, Inc.) The second generation lentiviral system plasmid plenti-CMV-MDM2-GFP-puro, pCMV-VSV-G (Addgene, Inc.) and pCMV-dR8.2 dvpr (Addgene, Inc.) (at a ratio of 4:1:3; 2 μg total plasmids) were co-transfected into 293T packaging cells. Additionally, plenti-CMV-puro empty vector (Addgene, Inc.), pCMV-VSV-G and pCMV-dR8.2 dvpr (at a ratio of 4:1:3; 2 μg total plasmids) were co-transfected into 293T packaging cells as a control group for control stable cell lines. All cells were cultured at 37˚C with 5% CO_2 for 8 h, and the media were replaced by fresh media. After 24 and 36 h, media were collected in centrifuge tubes. Subsequently, media were concentrated by ultracentrifugation at 16,100 x g for 30 min at 4˚C and filtered with a 4-μm filter. Viral titers were measured, and then recombinant lentiviral particles (10^7 TU/ml) were added to U251, A549 and MCF7 cells. The multiplicity of infection for U251, A549 and MCF7 cells was 3, 40 and 30, respectively. Equal volumes of complete media that contained 8 μg/ml Polybrene (Sigma-Aldrich; Merck KGaA) were then added. The media were replaced with fresh media containing 2 μg/ml Puromycin (Puro; Sigma-Aldrich; Merck KGaA) for selection after 24 h for stable cell line enrichment. The duration of the selection process was 7 days. Subsequently, complete media with 1 μg/ml Puro for maintenance were used to culture this purified stable cell line. Then, $2x10^5$ cells per well were seeded into six-well plates using 0.25% Trypsin-EDTA solution (Sigma-Aldrich; Merck KGaA) for 5 min at 37˚C, and then the stable cells were collected for qPCR and western blotting.

Western blot analysis. Cells were harvested in 1.5-ml microcentrifuge tubes and washed with PBS. Subsequently, Nonidet P (NP)-40 lysis buffer (2% NP-40, 80 mM NaCl, 100 mM Tris-HCl and 0.1% SDS) was added to the cells, and PMSF (1 mM; Thermo Fisher Scientific, Inc.) was supplemented. Cell lysate was incubated on ice for 5 min and then the lysate was centrifuged at 16,100 x g for 10 min at 4˚C. The sample protein concentration was determined using a Bio-Rad Protein DC Assay kit (Bio-Rad Laboratories, Inc.). Protein samples (50 μg per lane) from the control group and treatment group were subjected to SDS-PAGE (15%). Next, proteins were transferred from gels to a 0.45-μm PVDF membrane (EMD Millipore) at 200 mA for 70 min. The membranes were blocked with 5% BSA (Sigma-Aldrich; Merck KGaA) in PBS with 0.02% Tween 20 for 1 h at room temperature. Membranes were incubated with the primary antibodies (diluted to recommended concentration with 5% BSA) overnight at 4˚C. The antibodies used were as follows: Anti-GAPDH (rabbit; dilution, 1:1,000 for western blotting; cat no. 10494-1-AP; ProteinTech Group, Inc.), anti-GFP (mouse; dilution, 1:1,000 for western blotting; cat no. 66002-1-Ig; ProteinTech Group, Inc.), anti-p53 (mouse; dilution, 1:1,000 for western blotting; cat no. TA808657; OriGene Technologies, Inc.), phosphorylated (p-)B-Raf (dilution, 1:1,000 for western blotting; cat. no. 2696; Cell Signaling Technology, Inc.), B-Raf (dilution, 1:1,000 for western blotting; cat. no. 14814; Cell Signaling Technology, Inc.), p-MEK (dilution, 1:1,000 for western blotting; cat. no. 3958; Cell Signaling Technology, Inc.), MEK (dilution, 1:1,000 for western blotting; cat. no. 4694; Cell Signaling Technology, Inc.),

p-ERK (T202/Y204) (dilution, 1:1,000 for western blotting; cat. no. 4370; Cell Signaling Technology, Inc.), ERK (dilution, 1:1,000 for western blotting; cat. no. 4695; Cell Signaling Technology, Inc.), p-ribosomal protein S6 kinase (p70S6K) (T389) (dilution, 1:1,000 for western blotting; cat. no. 9206S; Cell Signaling Technology, Inc.), p70S6K (dilution, 1:1,000 for western blotting; cat. no. 9202S; Cell Signaling Technology, Inc.), p-eukaryotic translation initiation factor 4E binding protein 1 (4EBP1) (T37/46) (dilution, 1:1,000 for western blotting; cat. no. 9451T; Cell Signaling Technology, Inc.), 4EBP1(dilution, 1:1,000 for western blotting; cat. no. 9644S; Cell Signaling Technology, Inc.), 14-3-3 (pan) (dilution, 1:1,000 for western blotting; cat. no. 8312; Cell Signaling Technology, Inc.), E-CAD (dilution, 1:1,000 for western blotting; cat. no. 20874-1-AP; ProteinTech Group, Inc.), N-cadherin (N-CAD; dilution, 1:1,000 for western blotting; cat. no. GTX-127345; GeneTex, Inc.), vimentin (VIM; dilution, 1:1,000 for western blotting; cat. no. 5741T; Cell Signaling Technology, Inc.), zinc finger E-box binding homeobox 1 (ZEB1; dilution, 1:1,000 for western blotting; cat. no. 3396T; Cell Signaling Technology, Inc.), Snail (dilution, 1:1,000 for western blotting; cat. no. 3879T; Cell Signaling Technology, Inc.), Snail family transcriptional repressor 2 (Slug; dilution, 1:1,000 for western blotting; cat. no. 9585T; Cell Signaling Technology, Inc.), GFP (dilution, 1:1,000 for western blotting; cat. no. GTX-113617; GeneTex, Inc.) and Flag (dilution, 1:1,000 for western blotting; cat. no. F3165; Sigma-Aldrich; Merck KGaA). GAPDH served as a control. Then, appropriate anti-rabbit and anti-mouse secondary antibodies (cat nos. SA00001-1 and SA00001-2; ProteinTech Group, Inc.; dilution, 1:3,000 with 5% BSA) were added to the membranes for 1 h at room temperature. Subsequently, membranes were exposed to ECL solution (cat no. WBKLS0500; EMD Millipore) using an Amersham Imager 600 machine (GE Healthcare). For protein expression intensity measurement and quantification, densitometry of the bands was performed using ImageJ version 1.49 software (National Institutes of Health).

RNA extraction, cDNA synthesis and qPCR analysis. A RNeasy Mini kit (cat. no. 74104; QIAGEN Inc.) was used to extract total RNA of U251, MCF7 and A549 cells. The RNA products isolated using this kit were loaded on a 1% agarose gel and separated by electrophoresis. Subsequently, bands for 28S RNA, 18S RNA and 5S RNA were inspected to ensure that RNA was extracted correctly. Next, the RNA quality and concentration were assayed using a Nanodrop 2000 spectrophotometer (Thermo Fisher Scientific, Inc.). A total of 1 μg RNA was used for cDNA synthesis using the iScript™ cDNA Synthesis Kit (cat no. 170-8890; Bio-Rad Laboratories, Inc.). The reverse transcription (RT) conditions were as follows: 25°C for 5 min, 46°C for 20 min, 95°C for 60 sec, hold at 4°C. Primers used for qPCR are listed in Table I. PerfeCTa® SYBR® Green SuperMix (cat no. 95054-100; Quantabio) was used for qPCR and the conditions were as follows: 95°C for 3 min, 95°C for 15 sec, 55°C for 45 sec, 72°C for 30 sec, total of 35 cycles. A CFX96 Touch Real-Time PCR Detection System (Bio-Rad Laboratories, Inc.) was used to obtain and analyze the data. Actin was used to normalize gene expression levels. For quantification, the $2^{-\Delta\Delta Cq}$ method was used for this experiment (40).

Immunohistochemistry. Tissue sections were fixed in 10% neutral buffered formalin at room temperature for 48 h and then embedded in paraffin. The thickness of tissue sections was 4 μm. For immunohistochemical staining, slides were placed in a 65°C incubator for 30 min. Tissue slides were deparaffinized in xylene for 5 min, then in fresh xylene for another 5 min, 100% ethanol for 5 min, 95% ethanol for 5 min and 75% ethanol for 5 min, and then washed in water for 5 min. Endogenous peroxidase was blocked with 3% hydrogen peroxide. Antigen retrieval was achieved using a hot water bath (100°C) and 10 mM citric sodium buffer (pH 6.0) for 15 min. Sections were then blocked with 5% BSA for 1 h at room temperature and incubated overnight at 4°C with the indicated primary antibodies in 5% BSA: E-CAD (dilution, 1:100; cat. no. 20874-1-AP; ProteinTech Group, Inc.) and N-CAD (dilution, 1:50; cat. no. GTX-127345; GeneTex, Inc.). Antibody binding was detected using the EnVision™ Dual Link System-HRP DAB kit (undiluted; cat. no. K4010; Dako; Agilent Technologies, Inc.). Anti-Rabbit HRP labeled polymer (cat. no. K4010; Dako; Agilent Technologies, Inc.) was used to cover tissues, followed by incubation for 30 min at room temperature. Subsequently, 20 μl DAB (~1 drop) in 1 ml DAB substrate buffer was applied to each slide and incubated for 5 min. Sections were then counterstained with hematoxylin for 5 min at room temperature, followed by washing of the slides at room temperature. After staining, the slides were washed with running tap water for 5 min. Subsequently, tissue slides were placed in 75% ethanol for 5 min, 95% ethanol for 5 min, 100% ethanol for 5 min, xylene for 5 min and then in fresh xylene for another 5 min. For negative controls, primary antibodies were excluded. The mitotic index was quantified by viewing and capturing images of 10 random high-power fields for each tissue section on a Keyence All-In-One Fluorescence Microscope (Keyence Corporation), using a 40x or 20x objective. For evaluation and quantification of immunohistochemical data, 10 fields within the tumor area under high power magnification (40x) were randomly selected for evaluation using ImageJ version 1.49 software (National Institutes of Health). The investigators performed blind counting for all quantifications.

Clinical patient glioma samples. All clinical patient glioma samples were obtained from The Affiliated Hospital of Southwest Medical University (Luzhou, China). Recruitment was between March 2017 and May 2018. And the recruitment patient mean age is 33 years old. And all patient ages are among 18-59 years old. The recruitment patient proportion is 50 percent male and 50 percent female. The inclusion criteria were: i) Signature of informed consent voluntarily; ii) pathological diagnosis of glioma; iii) aged 18-59 years old, male and female; iv) normal blood-routine test; and v) normal liver function. The exclusion criteria were: i) Patients unwilling to participate in the experiment or had poor compliance; ii) other clinical trials being conducted; iii) previous history of brain tumor and radiotherapy conducted; iv) multiple lesions with extensive radiation volume; and v) with history of radiotherapy for brain tumors.

All samples were obtained from resection surgery and handled following clinical guidelines and in compliance with ethical standards (approval no. Y2019045; Southwest Medical

Table I. List of primers used for quantitative PCR.

Gene	Forward (5'-3')	Reverse (5'-3')
ACTIN	GCTCGTCGTCGACAACGGCT	CAAACATGATCTGGCTCATCTTCTC
E-CAD	CTGAGAACGAGGCTAACG	TTCACATCCAGCACATCC
ZEB1	GTGGCGGTAGATGGTAAT	CTGTTTGTAGCGACTGGA
SNAIL	CCCCAATCGGAAGCCTAA	CCTTTCCCACTGTCCTCAT
SLUG	TCCTGGTCAAGAAGCATT	GAGGAGGTGTCAGATGGA
MDM2	CGGGAGTCCGCAGTCTTA	GCTTGAGGGTCTGAATCTTG
VIMENTIN	CCAGGCAAAGCAGGAGTC	CGAAGGTGACGAGCCATT
N-CAD	CACTGCTCAGGACCCAGAT	TAAGCCGAGTGATGGTCC
P53	CACCCGCGTGCTAATGG	ATGCTGTGTGTACTCTGCTTGAACT

All these primers were designed for human genes. E-CAD, E-cadherin; H, human; MDM2, MDM2 proto-oncogene, E3 ubiquitin protein ligase; N-CAD, N-cadherin; ZEB1, zinc finger E-box binding homeobox 1.

University Ethics Committee, Luzhou, China). An informed consent document was signed by the patients to agree to the use of their samples in scientific research. Clinical samples were graded according to tumor cell density, mitotic index, degree of necrosis from the WHO Classification of Tumors (3rd Edition) (41). Samples were frozen at -196˚C in liquid nitrogen for qPCR, western blotting and paraffin sectioning for subsequent histological examination.

Clonogenic cell survival assay. After treatment (24 h exposure), cells were trypsinized, counted, and 800 cells per well were re-plated in six-well plates for colony formation assays. After incubation for 10-14 days, colonies were fixed with methanol:acetic acid (3:1; pre-cooled at 4˚C) at 4˚C for 10 min, and stained with 1% crystal violet at room temperature for 15 min, and then counted. A light microscope (Nikon Corporation) was used to observe and count colonies, and GraphPad Prism 6.0 software (GraphPad Software, Inc.) was used for quantification and analysis. Plating efficiency (PE) was determined, and the surviving fraction was calculated based on the number of colonies that arose after treatment and is expressed in terms of PE. Each experiment was repeated three times.

High throughput RNA sequencing (RNA-seq). RNA was prepared using the Qiagen RNeasy Kit (cat. no. 74104; Qiagen, Inc.) according to the manufacturer's protocols. Strand-specific libraries were generated using the KAPA Stranded mRNA-Seq Kit with KAPA mRNA Capture Beads (cat no. KK8421; Kapa Biosystems; Roche Diagnostics). Sequencing libraries were quantified using the Qubit 2.0 Fluorometer (Invitrogen; Thermo Fisher Scientific, Inc.) and validated using High-Performance Capillary Electrophoresis and the Agilent Tapestation 4200 (Agilent Technologies, Inc.). RNA-seq was performed by Genewiz, Inc. The sequencing libraries were multiplexed and clustered on one lane of a Flow Cell. After clustering, the Flow Cell was loaded on the Illumina HiSeq instrument (Illumina, Inc.) according to the manufacturer's protocol. The samples were sequenced using a 2x150 Paired End configuration. Image analysis and base-calling were conducted by the HiSeq Control Software

(version 3.3.20; Illumina, Inc.). Raw sequence data (.bcl files) generated from Illumina HiSeq were converted into Fastq files and de-multiplexed using Illumina's bcl2fastq software (version 2.17; Illumina, Inc.). One mismatch was allowed for index sequence identification. The quality of Fastq files was checked with FastQC (version 0.11.8; Baraham Bioinformatics group; http://www.bioinformatics.babraham.ac.uk/). To be referred to as 'differentially expressed', a gene had to have a false discovery rate adjusted P<0.05 in Differential Expression Analysis of RNA-seq Data (DEseq) as well as in null model of hypothesis. DesEQ2 performs a likelihood ratio test that compares how well a gene count data fits a full model (with independent variable time) compared with a reduced model without those variables. The null model of hypothesis takes the average expression of groups into consideration. The gene list was further ranked using fold change criteria.

Gene set enrichment analysis (GSEA). GSEA was used to study the enrichment of genes in different pathways. Non-parametric GSEA was performed using GSEA 3.0 (Broad Institute, Inc.; http://www.gsea-msigdb.org/gsea/index.jsp). The gene sets that significantly out-performed random-class permutations were considered significant.

MTT assay. Cells were digested and then seeded into 24-well culture plates at a density of $1x10^4$ cells/well. Subsequently, cells were treated with Silibinin at the indicated concentration for 24 and 48 h. MTT reagent (5 mg/ml; HyClone; Cytiva) was then added to each well, and the cells were incubated at 37˚C for 4 h. After incubation, DMSO was used to replace the MTT reagent, and cells were further incubated at room temperature for 30 min. The absorbance of formazan at 570 nm was detected using a spectrophotometer (Bio-Rad Laboratories, Inc.).

Scratch wound migration assay. U251 and A549 cells were first seeded into a 12-well cell culture plate ($2x10^5$ cells/well). The monolayer was scratched using a 200-μl pipet tip when the cell confluence reached 75-80%. Subsequently, cells were cultured in an incomplete medium that contained 0.5% serum. Images were captured at 0, 24 and 48 h after wounding using a

light microscope (Olympus Corporation). ImageJ (version 1.49; National Institutes of Health) was used to analyze these images, and the cell migration ratio was calculated as follows: $N=[1-(D_n/D_0)] \times 100\%$, where N represents the ratio of cell migration, D_n represents the closure distance at the sampling time and D_0 represents the original distance.

Animal experiments. NOD/SCID mice (stock no. 001303) were purchased from Chengdu Dossy Experimental Animals Co., Ltd. All animal experiments were performed following the guidelines that were reviewed and approved by Southwest Medical University Ethics Committee (Luzhou, China) before conduction (approval no. 201903-34). For subcutaneous xeno-grafts, U251 cells and stable MDM2 and 14-3-3-expressing cells (5×10^6) in PBS were injected subcutaneously into the lower flank of 6-week-old female NOD/SCID mice (weight, ~20 g; 6 mice per group; total of 24 mice). All mice were housed in a SPF mice room under standard conditions (temperature, 20-26˚C; humidity, 40-70%; ammonia concentration below 14 mg/m^3; light/dark cycle was 12/12 h; free access to food and water). Animal health and behavior were monitored daily. Mice were monitored for tumor development by measure-ments of tumor weight, tumor length and width. Tumor volume was calculated according to the following formula: (Length x width^2)/2. Related mice were treated daily with 100 mg/kg (body weight) FR180204 via intraperitoneal injection using a 27-gauge needle. The duration of the experiment was 28 days. After a 4-week period (post-inoculation), once tumors grew to a palpable size (~500 mm^3), the mice were sacrificed (no mice died before the endpoint), and tumors were dissected (no other tumors were observed). To minimize the struggle of the animals and reduce the pain of the animal, the cervical disloca-tion method was performed after the mice were anesthetized. When mice were sacrificed, mice were placed in the induction chamber with 2% isoflurane (induction dose) in oxygen, and then cervical dislocation was used for euthanasia immediately. Half of each tumor was frozen at -196˚C in liquid nitrogen, and half was fixed in 4% paraformaldehyde for subsequent histological examinations.

During the 4-week observation period, if there was evidence of weight loss >20% from the baseline, partial rigor of the limbs, inability to regain normal posture if placed on back, labored breathing, inability to eat or drink, severe dyspnea or any other serious illness, the mice would have been euthanized. Consequently, tumor growth of 1.0 cm^3 will be a humane endpoint to euthanize mice. Mice would be euthanized if tumor growth plateaus for more than five measurements in which case controls would be concurrently euthanized with experimental populations. Animals were checked daily for body condition scoring and signs of discomfort. Those animals in pain or extreme discomfort would have been euthanized. The final decision to perform euthanasia was at the discretion of the clinical veterinarian.

Image capture and analysis. Images were acquired using Olympus Stream software (version 2.4; Olympus Corporation) under a fluorescence microscope (Olympus Corporation), and ImageJ (version 1.49; National Institutes of Health) was used to analyze the images. Band densitometry and data quanti-fication was also conducted using ImageJ. All images in the present study were grouped using Adobe Illustrator software (version 24.0; Adobe Systems, Inc.).

Statistical analysis. Data were normalized using control markers. Data from each group were obtained from at least three replicates. Mean values and SD are presented. In this study, statistical analysis was performed using GraphPad Prism 6.0 software (GraphPad Software, Inc.). Statistical significance was analyzed using an unpaired Student's t-test or one-way ANOVA with Tukey's post hoc test to correct for multiple comparisons. $P<0.05$ was considered to indicate a statistically significant difference, $P<0.01$ was considered to indicate a statistically very significant difference and $P<0.001$ was considered to indicate a statistically extremely significant difference.

Results

MDM2 expression is increased in TGF-β-induced EMT. According to previous studies, MDM2 is an important factor related to cell invasion, metastasis and EMT (7,8). Therefore, the present study aimed to determine the MDM2 levels in cells undergoing EMT. TGF-β can induce EMT (6). U251 cells were incubated with 10 ng/ml TGF-β or an equal volume of 20 mM Citrate solution buffer which was the buffer solution for TGF-β. Subsequently, cells were collected and total RNA was extracted. As shown in Fig. 1A, compared with the control group, full length MDM2 was upregulated ~2.5 times after incubation based on semi-quantitative analysis of band inten-sity from PCR results. Similarly, MDM2 gene expression in U251 cells treated in the same manner was increased ~3 times after incubation according to qPCR (Fig. 1B). Subsequently, the protein expression levels of MDM2, p53, E-CAD, N-CAD and VIM in TGF-β-treated U251 cells were analyzed by western blotting (Fig. 1C). As shown in the quantitative analyses, U251 cells treated with TGF-β exhibited decreased E-CAD protein expression and increased N-CAD and VIM protein expression, which suggested that EMT had been induced. In the same cells, RT-qPCR indicated that the *MDM2* expression was significantly increased after incubation with TGF-β peptide (Fig. 1D). Furthermore, since MDM2 is an upstream gene of p53, the present study also determined p53 protein expression (2-4). Consistent with other publications, it was observed that the accumulation of MDM2 was associated with the degradation of p53 (Fig. 1C). To summarize, MDM2 expression was upregulated in EMT induced by TGF-β.

MDM2 overexpression induces EMT in U251 glioma cells. The aforementioned results demonstrated that MDM2 expres-sion was upregulated by TGF-β-induced EMT. Furthermore, a previous study has reported that MDM2 can promote EMT in breast cancer cells (42). Therefore, clinical glioma samples were collected from patients with different patho-logical gradings. These tumor samples were then processed for immunohistochemistry. According to the immunohisto-chemistry results and positive cell quantification data, it was identified that the higher the glioma grading, the higher the protein expression levels of MDM2 (Fig. 2A). Additionally, the present study used qPCR and western blotting to analyze MDM2 gene and protein expression, respectively, in tumor
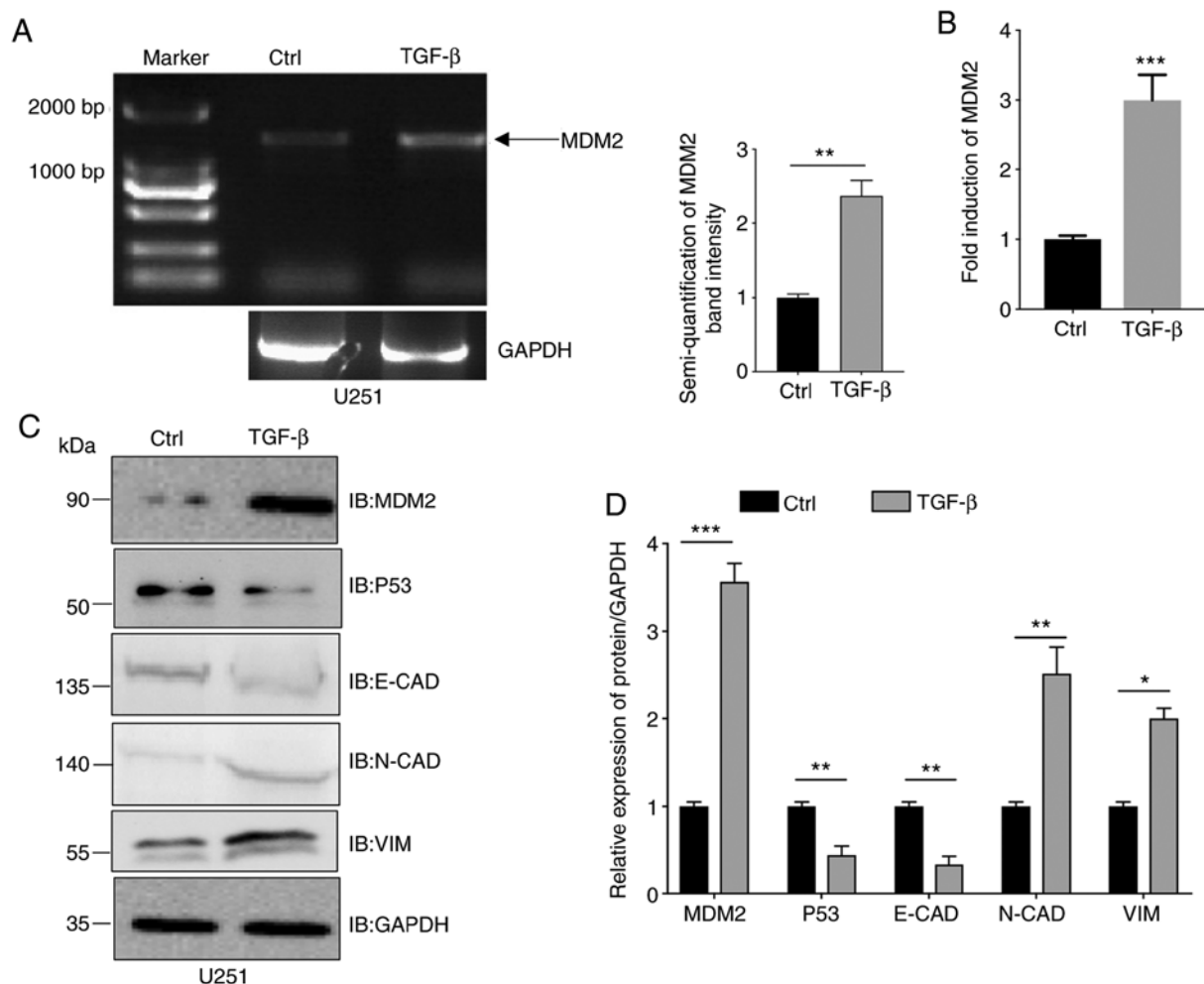
Figure 1. MDM2 expression is upregulated in TGF-β-induced epithelial-to-mesenchymal transition. (A) U251 cells were incubated with 10 ng/ml TGF-β for 72 h and MDM2 expression was analyzed by semi-quantitative reverse transcription PCR. The control group was incubated with an equal volume buffer solution in the U251 cell line. *GAPDH* was used as a control. (B) U251 cells were incubated with 10 ng/ml TGF-β for 72 h and the MDM2 expression was analyzed by quantitative PCR. *GAPDH* was used as a control. (C) MDM2, p53, E-CAD, N-CAD and VIM protein expression was analyzed by western blotting in U251 cells treated with 10 ng/ml TGF-β for 72 h. GAPDH was used as a loading control. (D) Semi-quantitative analysis of the expression levels of MDM2, E-CAD, N-CAD, VIM and p53 in U251 cells treated with 10 ng/ml TGF-β for 72 h. GAPDH was used as a control. For all quantifications, data are presented as the mean ± SD derived from three independent experiments. Comparisons were made using Student's t-test. $^*P<0.05$; $^{**}P<0.01$; $^{***}P<0.001$. The control group was the U251 cell line, which was incubated with an equal volume of buffer solution. Ctrl, control; E-CAD, E-cadherin; IB, immunoblotting; MDM2, MDM2 proto-oncogene, E3 ubiquitin protein ligase; N-CAD, N-cadherin; VIM, vimentin.

samples. Similar to the immunohistochemistry findings, it was observed that the expression levels of MDM2 were positively associated with pathological grade. MDM2 expression in G3 glioma samples was the highest, and it was the lowest in G1 glioma samples (Fig. 2B-D). It is well known that higher tumor pathological grades are strongly associated with higher malignancy and lower tumor differentiation, which results in higher metastatic potential (6,7). EMT is an important mechanism enabling tumor metastasis (6-8). The present data suggested that MDM2 may serve a key role in inducing EMT in glioma. Therefore, the present study aimed to determine whether MDM2 overexpression could induce EMT in U251 cells. pLenti-CMV-MDM2-GFP-puro (Fig. S1A) was a flexible and convenient tool for studying MDM2 expression by tracking green fluorescence by microscopy. Recombinant lentiviral plasmid (pLenti-CMV-MDM2-GFP-puro) was co-transfected into 293T packaging cells to generate MDM2-GFP lentivirus. In the control group, empty vector pLenti-CMV-Puro was

used. After 36 h, green fluorescence was observed (Fig. S1C), and the virus was then collected and concentrated by ultra-centrifugation. Viral titers were measured, and then the virus was added to U251 cells. After purification, green fluorescence was observed in stable puro positive U251 cells (Fig. S1D). Stable control U251 cells and stable U251 cells overexpressing MDM2-GFP were collected, and total RNA was extracted. The gene expression levels of *MDM2*, *p53*, *E-CAD, N-CAD* and *VIM* were analyzed (Fig. 2E). Subsequently, band intensity was quantified by SqRT-PCR (Fig. 2E). As shown by the quantification data, MDM2 overexpression significantly decreased the gene expression levels of *E-CAD* and significantly increased the gene expression levels of *N-CAD* and *VIM* at the same time. This suggested that EMT had been successfully induced compared with the control group (Fig. 2E and F). qPCR was also used to verify these in stable control U251 cells and stable U251 cells overexpressing MDM2-GFP (Fig. 2F). p53 gene expression was also decreased significantly compared with the
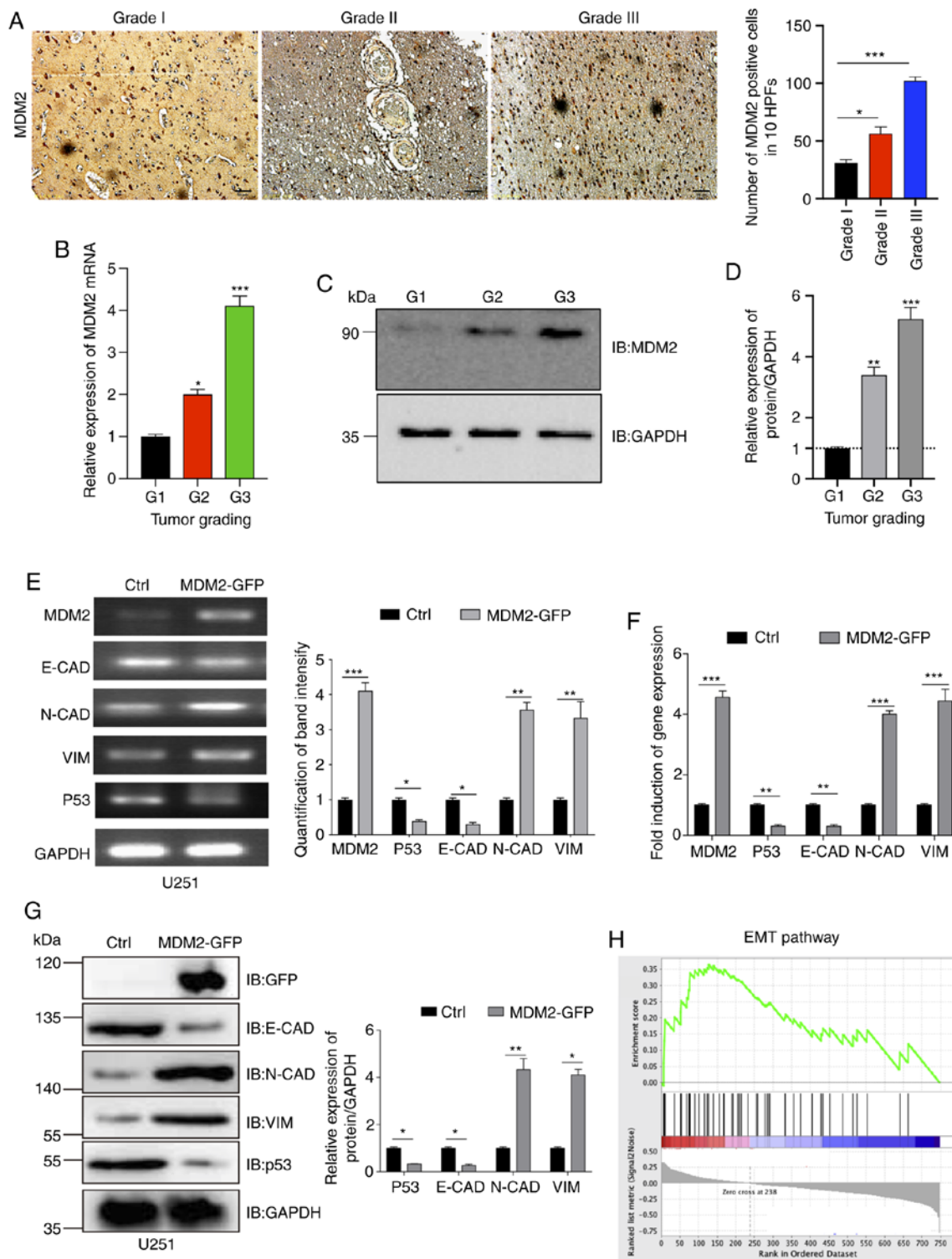
Figure 2. MDM2 overexpression induces EMT in U251 cells. (A) Immunohistochemical staining of MDM2 and quantification of positive MDM2 cells in 10 HPFs. Data are from clinical patient glioma samples that represented 5-6 patients from each group. Scale bars, 50 μm. (B) qPCR analyses of MDM2 expression in indicated clinical patient glioma samples (three randomly selected samples per group). *GAPDH* served as a control. (C) Immunoblot analyses of MDM2 expression in indicated clinical patient glioma samples. GAPDH served as a loading control. (D) Densitometric quantitation of the relative expression levels of the MDM2 protein in the clinical patient glioma samples. n=3 independent experiments. (E) *MDM2*, *p53* and EMT levels were analyzed by semi-quantitative reverse transcription PCR. Ctrl referred to the U251 cell line with stable overexpression of plenti-CMV-puro empty vector. *GAPDH* was used as a control. (F) *MDM2*, *p53* and *E-CAD*, *N-CAD* and *VIM* expression was analyzed by qPCR. Ctrl referred to the U251 cell line with stable overexpression of plenti-CMV-puro empty vector. (G) Immunoblot analyses and semi-quantitative analysis of the expression levels of MDM2, E-CAD, N-CAD, VIM and p53 in stable MDM2 overexpression cells and control cells. Ctrl referred to the U251 cell line with stable overexpression of plenti-CMV-puro empty vector. (H) Gene Set Enrichment Analysis plot for U251 cells showing the most significantly changed EMT pathway gene set. Note that the EMT gene signature was significantly upregulated upon expression of MDM2 but downregulated upon expression of empty vector. For all quantifications, data are presented as the mean ± SD derived from three independent experiments. Statistical significance was analyzed using an unpaired Student's t-test in (E, F and G) Statistical significance was analyzed using one-way ANOVA with Tukey's post hoc test to correct for multiple comparisons in (A, B and D). *P<0.05; **P<0.01; ***P<0.001 vs. G1 or as indicated. Ctrl, control; E-CAD, E-cadherin; EMT, epithelial-to-mesenchymal transition; GFP, green fluorescent protein; HPFs, high-power fields; IB, immunoblotting; MDM2, MDM2 proto-oncogene, E3 ubiquitin protein ligase; N-CAD, N-cadherin; qPCR, quantitative PCR; VIM, vimentin.
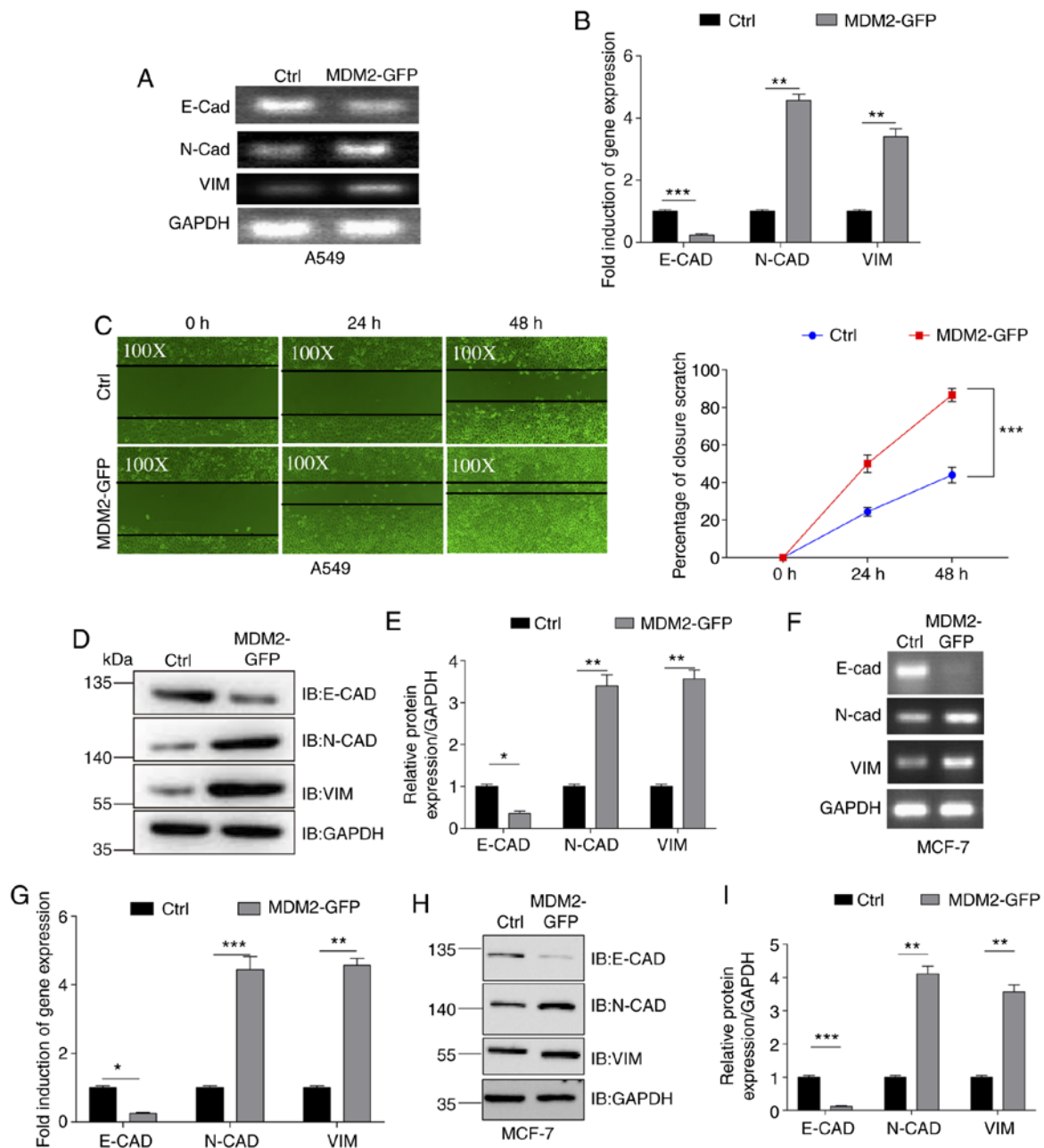
Figure 3. MDM2 overexpression induces EMT in A549 and MCF7 cells. (A) EMT levels were analyzed by SqRT-PCR. *GAPDH* served as a control. Ctrl referred to the A549 cell line with stable overexpression of plenti-CMV-puro empty vector. (B) *E-CAD, N-CAD* and *VIM* levels were analyzed by qPCR in a A549 stable cell line. Ctrl referred to the A549 cell line with stable overexpression plenti-CMV-puro empty vector. *GAPDH* served as a control. (C) Migration of MDM2-GFP-overexpressing A549 cells (magnification, x100) and control cells (magnification, x100) at 0, 24 and 48 h after wounding. Data are presented as the percentage closure of each scratch at 0, 24 and 48 h after wounding. MDM2 overexpression significantly induced cell migration in A549 cells. Ctrl referred to the A549 cell line with stable overexpression of plenti-CMV-puro empty vector. (D) E-CAD, N-CAD and VIM levels were analyzed by western blotting in a MDM2-overexpressing A549 stable cell line and A549 control cells. Ctrl referred to the A549 cell line with stable overexpression of plenti-CMV-puro empty vector. (E) Semi-quantification of the relative expression levels of the E-CAD, N-CAD and VIM levels in a MDM2-overexpressing A549 stable cell line and A549 control cells. n=3 independent experiments. Ctrl referred to the A549 cell line with stable overexpression of plenti-CMV-puro empty vector. (F) EMT levels were analyzed by SqRT-PCR in MCF7 stable cell lines. Ctrl referred to the MCF7 cell line with stable overexpression of plenti-CMV-puro empty vector. *GAPDH* served as a control. (G) *E-CAD, N-CAD* and *VIM* levels were analyzed by qPCR in MCF7 stable cell lines. Ctrl referred to the MCF7 cell line with stable overexpression of plenti-CMV-puro empty vector. *GAPDH* served as a control. (H and I) E-CAD, N-CAD and VIM expression was analyzed by western blotting in MCF7 stable cell lines. Ctrl referred to the MCF7 cell line with stable overexpression of plenti-CMV-puro empty vector. For all quantifications, data are presented as the mean ± SD derived from three independent experiments. Comparisons were made using Student's t-test. *P<0.05; **P<0.01; ***P<0.001. Ctrl, control; E-CAD, E-cadherin; EMT, epithelial-to-mesenchymal transition; GFP, green fluorescent protein; IB, immunoblotting; MDM2, MDM2 proto-oncogene, E3 ubiquitin protein ligase; N-CAD, N-cadherin; qPCR, quantitative PCR; SqRT-PCR, semi-quantitative reverse transcription PCR; VIM, vimentin.

control group due to the degradation of p53 by MDM2 overexpression (Fig. 2E and F). MDM2, p53, E-CAD, N-CAD and VIM protein expression in stable control U251 cells and stable

U251 cells overexpressing MDM2-GFP was then analyzed by western blotting. Consistent with the gene expression data, MDM2 overexpression significantly decreased the protein
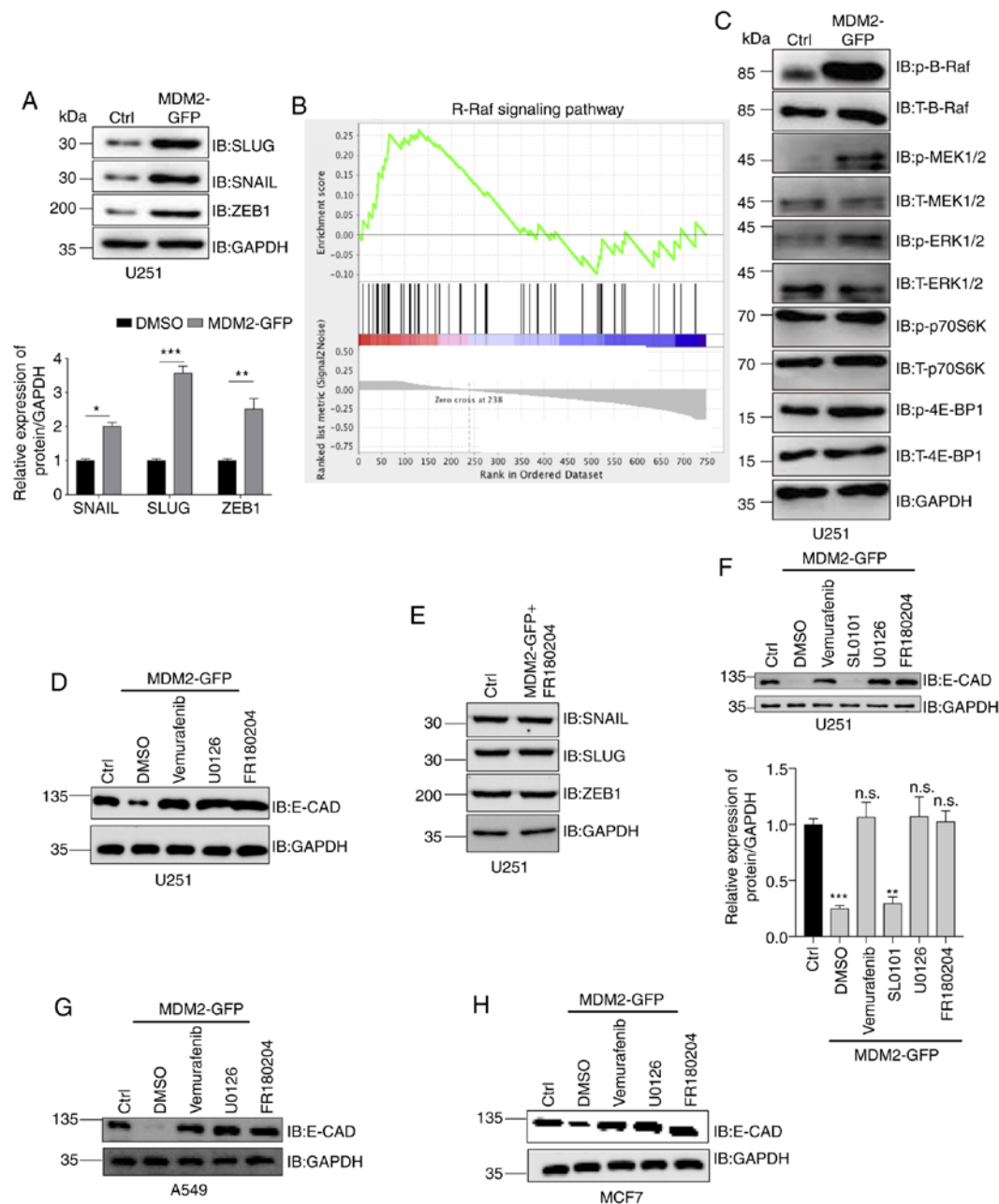
Figure 4. MDM2 induces epithelial-to-mesenchymal transition progression via the B-Raf signaling pathway. (A) Snail, Slug and ZEB1 expression was analyzed by western blotting in stable MDM2-overexpressing U251 cells and control U251 cells. Ctrl referred to the U251 cell line with stable overexpression of plenti-CMV-puro empty vector. GAPDH was used as a control, and semi-quantitative analysis is shown. (B) Gene Set Enrichment Analysis plot of U251 cells showing the most significantly changed B-Raf signaling pathway set. Note that the B-Raf signaling pathway was significantly upregulated upon expression of MDM2 but downregulated upon expression of empty vector. (C) Western blot analysis of the levels of p-B-Raf, p-MEK, p-ERK, p-P70S6K and p-4EBP1 in stable MDM2-overexpressing U251 cells and control U251 cells. Ctrl referred to the U251 cell line with stable overexpression of plenti-CMV-puro empty vector. GAPDH served as a control. (D) E-CAD levels were analyzed by western blotting in control U251 cells and stable MDM2-overexpressing U251 cells following treatment with DMSO, vemurafenib (B-Rafi at 2 μM for 24 h), U0126 (MEKi at 20 μM for 24 h) and FR180204 (ERKi at 10 μM for 24 h). Ctrl referred to the U251 cell line with stable overexpression of plenti-CMV-puro empty vector. GAPDH was used as a control. (E) Snail, Slug and ZEB1 levels were analyzed by western blotting in control U251 cells and stable MDM2-overexpressing U251 cells treated with FR180204 (ERKi at 10 μM for 24 h). Ctrl referred to the U251 cell line with stable overexpression of plenti-CMV-puro empty vector. GAPDH was used as a normalization control. (F) E-CAD expression was analyzed by western blotting in stable control U251 cells and stable MDM2-overexpressing U251 cells treated with Vemurafenib, U0126, FR180204 and SL0101 (RSKi at 50 μM for 24 h). Ctrl referred to the U251 cell line with stable overexpression of plenti-CMV-puro empty vector. GAPDH was used as a control, and the band density was semi-quantified. (G) E-CAD expression was analyzed by western blotting in stable control A549 cells and stable MDM2-overexpressing A549 cells treated with DMSO, vemurafenib (B-Rafi at 2 μM for 24 h), U0126 (MEKi at 20 μM for 24 h), and FR180204 (ERKi at 10 μM for 24 h). Ctrl referred to the A549 cell line with stable overexpression of plenti-CMV-puro empty vector. GAPDH was used as a control. (H) E-CAD levels were analyzed by western blotting in stable control MCF7 cells and stable MDM2-overexpressing MCF7 cells treated with DMSO, vemurafenib (B-Rafi at 2 μM for 24 h), U0126 (MEKi at 20 μM for 24 h) or FR180204 (ERKi at 10 μM for 24 h). Ctrl referred to the MCF7 cell line with stable overexpression of plenti-CMV-puro empty vector. GAPDH was used as a control. For all quantifications, data are presented as the mean ± SD derived from three independent experiments. Statistical significance was analyzed using an unpaired Student's t-test for A, and one-way ANOVA with Tukey's post hoc test was used to compare the indicated group and Ctrl in F. *P<0.05; **P<0.01; ***P<0.001; n.s., not significant vs. Ctrl or as indicated. 4EBP1, eukaryotic translation initiation factor 4E binding protein 1; BRafi, B-Raf inibibor; Ctrl, control; E-CAD, E-cadherin; ERKi, ERK inhibitor; GFP, green fluorescent protein; IB, immunoblotting; MDM2, MDM2 proto-oncogene, E3 ubiquitin protein ligase; MEKi, MEK inhibitor; p-, phosphorylated; P70S6K, ribosomal protein S6 kinase; RSKi, RSK inhibitor; Slug, Snail family transcriptional repressor 2; Snail, Snail family transcriptional repressor 1; T-, total; ZEB1, zinc finger E-box binding homeobox 1.

expression levels of E-CAD and p53, and markedly increased the protein expression levels of N-CAD and VIM (Fig. 2G). MDM2 overexpression and control U251 cell lines were then used for RNA-Seq. GSEA revealed that the EMT pathway gene set was closely associated with the expression levels of MDM2 compared with the control group (Fig. 2H). Overall, MDM2 overexpression could induce EMT in U251 cells.

MDM2 overexpression induces EMT in A549 and MCF7 cancer cells. The aforementioned results demonstrated that overexpression of MDM2 could promote EMT in the U251 glioma cell line. Subsequently, the present study examined whether MDM2 overexpression induced EMT in other cancer cell lines. Lentivirus from 293T cells was added to the A549 lung cancer cell line to yield control A549 cells and A549 cells stably overexpressing MDM2-GFP. Green fluorescence was observed in stable A549 cells after purification (Fig. S1E), and the gene and protein expression levels of MDM2-GFP were assessed by qPCR (Fig. S2A) and western blotting (Fig. S2B). Subsequently, the gene expression levels of *E-CAD*, *N-CAD* and *VIM* were determined by SqRT-PCR and qPCR in these two stable A549 cell lines (Fig. 3A and B). As shown in the quantification analysis, MDM2 overexpression significantly decreased the gene expression levels of *E-CAD* and significantly increased the gene expression levels of *N-CAD* and *VIM*. Furthermore, the migration ability of these two stable cell lines was determined. Scratch wound assays were used to evaluate their migration abilities and the percentage closure of the scratch wound was quantified at 0, 24 and 48 h post injury in these two cell lines (Fig. 3C). As shown by the images of migration and quantification data, the percentage closure in the MDM2 overexpression group was higher than that in the control group at 24 and 48 h post injury (Fig. 3C). These data demonstrated that MDM2 overexpression increased the cell migration abilities of A549 cells. Additionally, E-CAD, N-CAD and VIM protein expression was analyzed by western blotting (Fig. 3D and E). Consistently, MDM2 overexpression significantly decreased the protein expression levels of E-CAD and significantly increased the protein expression levels of N-CAD and VIM (Fig. 3D and E). Therefore, the present data demonstrated that MDM2 overexpression induced EMT in the A549 lung cancer cell line. Furthermore, this was also tested in the MCF7 breast cancer cell line. Green fluorescence was observed in stable MCF7 cells after purification (Fig. S1F), and gene and protein expression levels of MDM2-GFP were assessed by qPCR (Fig. S2C) and western blotting (Fig. S2D). According to SqRT-PCR, qPCR and western blotting data, MDM2 overexpression also induced EMT in MCF7 cells (Fig. 3F-H). Therefore, overexpression of MDM2 promoted EMT in a number of cancer cell lines.

MDM2 induces EMT by activating B-Raf signaling. Previously, it was demonstrated that MDM2 promoted EMT in glioma cells (U251), lung cancer cells (A549) and breast cancer cells (MCF7). However, the mechanism by which MDM2 induced EMT was not clear. Therefore, the present study aimed to determine the mechanism driving this EMT. It was previously identified that the protein expression levels of E-CAD, N-CAD and VIM were altered, and the gene levels were also altered. This suggested that the transcription factors that control EMT

may have been upregulated when MDM2 was overexpressed. Snail, Slug and ZEB1 are the most important transcriptional factors of EMT (Fig. 4A) (6,43,44). Therefore, Snail, Slug and ZEB1 protein expression was analyzed by western blotting in stable MDM2-overexpressing U251 cells and control U251 cells. As shown in the semi-quantification data, MDM2 overexpression significantly upregulated the protein expression levels of Snail, Slug and ZEB1 (Fig. 4A). Since these transcription factors were activated, the present study aimed to determine the upstream signaling pathway driving their upregulation. Therefore, GSEA was used to analyze these two stable cell lines, and revealed that the gene set for the B-Raf signaling pathway was closely associated with MDM2 expression compared with the control group (Fig. 4B). Additionally, GSEA was used to analyze whether the mTOR signaling pathway was associated with the expression levels of MDM2. However, according to the present data, no significant association was observed between the mTOR signaling pathway and MDM2 overexpression in U251 cells (data not shown). Subsequently, western blotting was used to analyze the levels of p-B-Raf, p-MEK and p-ERK to verify whether the B-Raf signaling pathway was activated by MDM2 overexpression. Consistent with the present GSEA data, western blotting demonstrated that the B-Raf signaling pathway was activated (Fig. 4C). Furthermore, the levels of p-P70S6K and p-4EBP1, downstream target genes of mTOR, were determined by western blotting (45-47). No significant changes in the levels of p-P70S6K and p-4EBP1 were detected, indicating that this process was independent of the mTOR signaling pathway (Fig. 4C). E-CAD levels were also analyzed by western blotting in stable control U251 cells and stable U251 cells overexpressing MDM2-GFP following treatment with DMSO, vemurafenib (B-Raf inhibitor) (48,49), U0126 (MEK inhibitor) (50,51) and FR180204 (ERK inhibitor) (52,53). As shown in Fig. 4, vemurafenib, U0126 and FR180204 could prevent the decrease in the protein expression of E-CAD (Fig. 4D and F). However, RSK inhibitor SL0101 did not affect the protein expression of E-CAD (Fig. 4D and F), which suggested that inhibition of B-Raf signaling could prevent MDM2 from inducing EMT. In other words, MDM2 promoted EMT by activating the B-Raf signaling pathway. Subsequently, the protein expression levels of Snail, Slug and ZEB1 were analyzed by western blotting in MDM2-overexpressing U251 cells which were treated with FR180204 and in control U251 cells (U251 cell line with stable overexpression of plenti-CMV-puro empty vector). No significant changes in the expression levels of Snail, Slug or ZEB1 were detected between the two groups by western blotting, which suggested that ERK inhibition could inhibit the increase of these EMT transcription factors (Fig. 4E). These data verified that MDM2 induced EMT by upregulating EMT transcription factors via the B-Raf signaling pathway. Additionally, the present data demonstrated that B-Raf inhibitors, MEK inhibitors and ERK inhibitors could all rescue the protein expression levels of E-CAD. RSK is a downstream protein kinase of ERK (54,55). To determine whether components downstream of ERK also participated in this process, western blotting was used to analyze E-CAD protein expression in control U251 cells and MDM2-overexpressing U251 cells treated with SL0101 (RSK inhibitor). As shown in the western blot images and semi-quantification data, only the
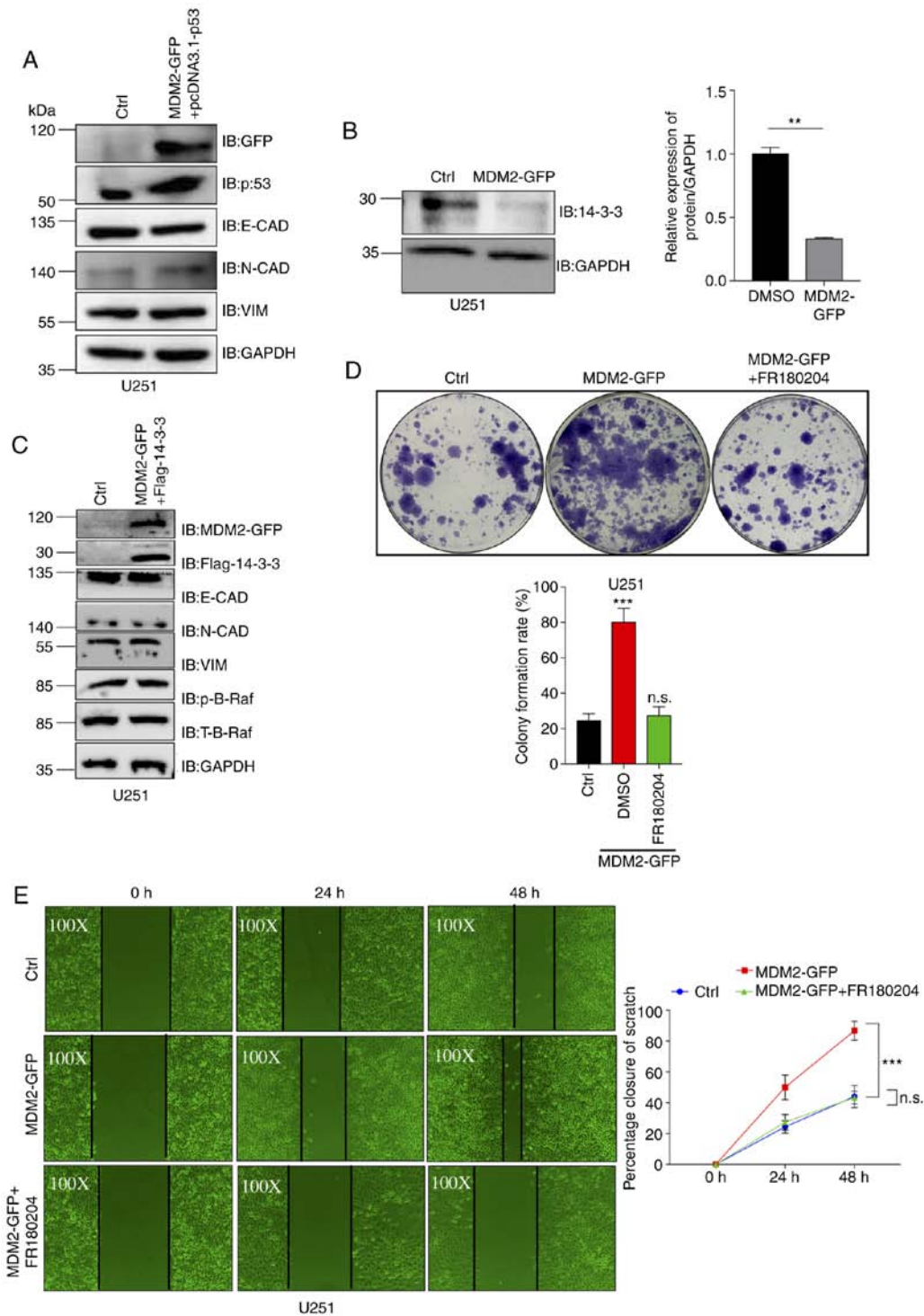
Figure 5. MDM2-mediated B-Raf signaling pathway activation via 14-3-3 is dependent on p53. (A) MDM2, p53, E-CAD, N-CAD and VIM protein expression was analyzed by western blotting in control U251 cells and stable MDM2-overexpressing U251 cells transfected with pcDNA3.1-p53. Ctrl referred to the U251 cell line with stable overexpression of plenti-CMV-puro empty vector. GAPDH was used as a control. (B) Western blot analysis of the expression levels of 14-3-3 in stable MDM2-overexpressing U251 cells and control U251 cells. Ctrl referred to the U251 cell line with stable overexpression of plenti-CMV-puro empty vector. GAPDH was used as a control. Semi-quantitative analysis data are shown. (C) MDM2, 14-3-3, E-CAD, N-CAD, VIM and p-B-Raf protein expression was analyzed by western blotting in control U251 cells and stable MDM2-overexpressing U251 cells expressing Flag-14-3-3. Ctrl referred to the U251 cell line with stable overexpression of plenti-CMV-puro empty vector. GAPDH was used as a control. (D) Colony formation assay for control U251 cells, stable MDM2-overexpressing U251 cells and stable MDM2-overexpressing U251 cells treated with FR180204 (ERKi at 10 μM). Ctrl referred to the U251 cell line with stable overexpression of plenti-CMV-puro empty vector. Data are presented as the mean ± SD percentage of colonies for each group after 14 days (bottom). n=3 independent experiments. (E) Images of the migration of control U251 cells (magnification, x100), stable MDM2-GFP overexpressing U251 cells (magnification, x100) and stable MDM2-GFP-overexpressing U251 cells treated with FR180204 (ERKi at 10 μM) (magnification, x100) at 0, 24 and 48 h after wounding. MDM2 could induce cell migration in U251 cells and FR180204 treatment could rescue this cell migration in scratch wound assays. Ctrl referred to the U251 cell line with stable overexpression of plenti-CMV-puro empty vector. For all quantifications, data are presented as the mean ± SD derived from three independent experiments. Statistical significance was analyzed using an unpaired Student's t-test in B, and one-way ANOVA with Tukey's post hoc test was used to compare the indicated group and Ctrl or two indicated groups in D and E. **P<0.01; ***P<0.001; n.s., not significant vs. Ctrl or as indicated. 14-3-3, tyrosine 3-monooxygenase activation protein ε; Ctrl, control; E-CAD, E-cadherin; ERKi, ERK inhibitor; GFP, green fluorescent protein; IB, immunoblotting; MDM2, MDM2 proto-oncogene, E3 ubiquitin protein ligase; N-CAD, N-cadherin; p-, phosphorylated; T-, total; VIM, vimentin.
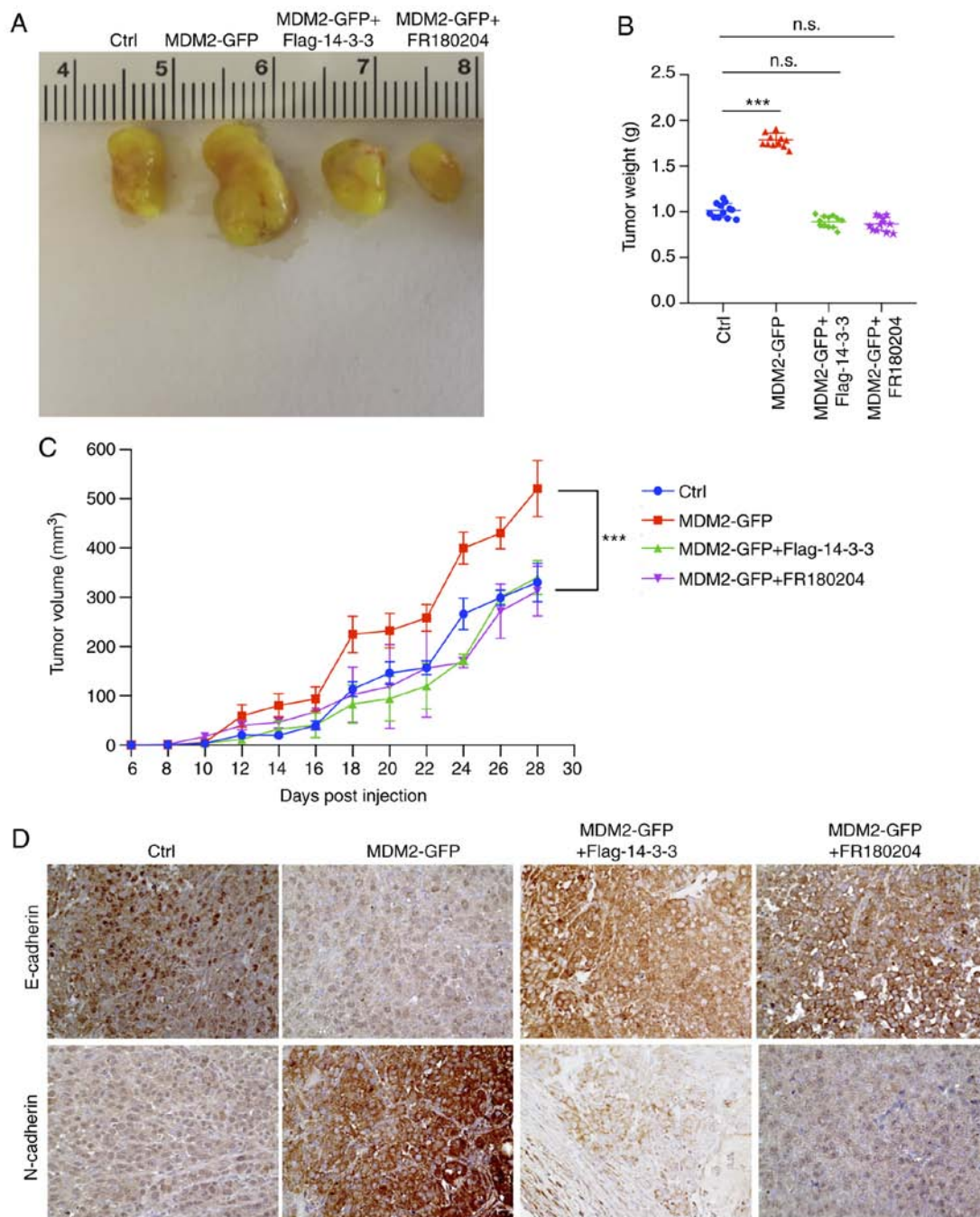
Figure 6. B-Raf signaling, which is activated by MDM2, can promote glioma xenograft tumor progression. (A) Representative images of tumors of NOD/SCID mice bearing U251 xenografts stably expressing empty vector, MDM2, MDM2 together with 14-3-3 or MDM2 together with an ERK inhibitor. Tumors isolated on day 28 after subcutaneous injection. Ctrl referred to tumors, which were injected with the stable overexpression of plenti-CMV-puro empty vector U251 cell line. Data are from one representative animal of 5-6 animals from each group. (B) Tumor weight from experiment in (A) upon autopsy at day 28 post injection. Ctrl referred to tumors, which were injected with the stable overexpression of plenti-CMV-puro empty vector U251 cell line. Results are presented as the mean weight (g) $\pm$ SD for 5-6 mice per group. (C) Tumor volume of xenografts formed after subcutaneous injection of NOD/SCID mice with U251 cells stably expressing indicated plasmids. Ctrl referred to tumors, which were injected with the stable overexpression of plenti-CMV-puro empty vector U251 cell line. Results are presented as the mean volume $\pm$ SD for 5-6 mice per group per time point. (D) Immunohistochemical staining of E-cadherin and N-cadherin in indicated U251 xenograft tumor genotypes (magnification, x400). Data are from 1 animal that was representative of the 5-6 animals from each group (n=5-6 mice per group). Ctrl referred to tumors, which were injected with the stable overexpression of plenti-CMV-puro empty vector U251 cell line. For all quantifications, data are presented as the mean $\pm$ SD derived from three independent experiments. Comparisons were made using Student's t-test. ***P<0.001; n.s., not significant. 14-3-3, tyrosine 3-monooxygenase activation protein ε; Ctrl, control; GFP, green fluorescent protein; MDM2, MDM2 proto-oncogene, E3 ubiquitin protein ligase.

RSK inhibitor had no effect on the protein expression levels of E-CAD (Fig. 4F), while all other drugs did have an effect. These data demonstrated that MDM2 induced EMT by upregulating EMT transcription factors via activation of ERK rather than through the ERK signaling pathway. Additionally, this mechanism was assessed in other cell lines, and E-CAD levels were analyzed by western blotting in control A549 cells and MDM2-overexpressing A549 cells treated with DMSO,
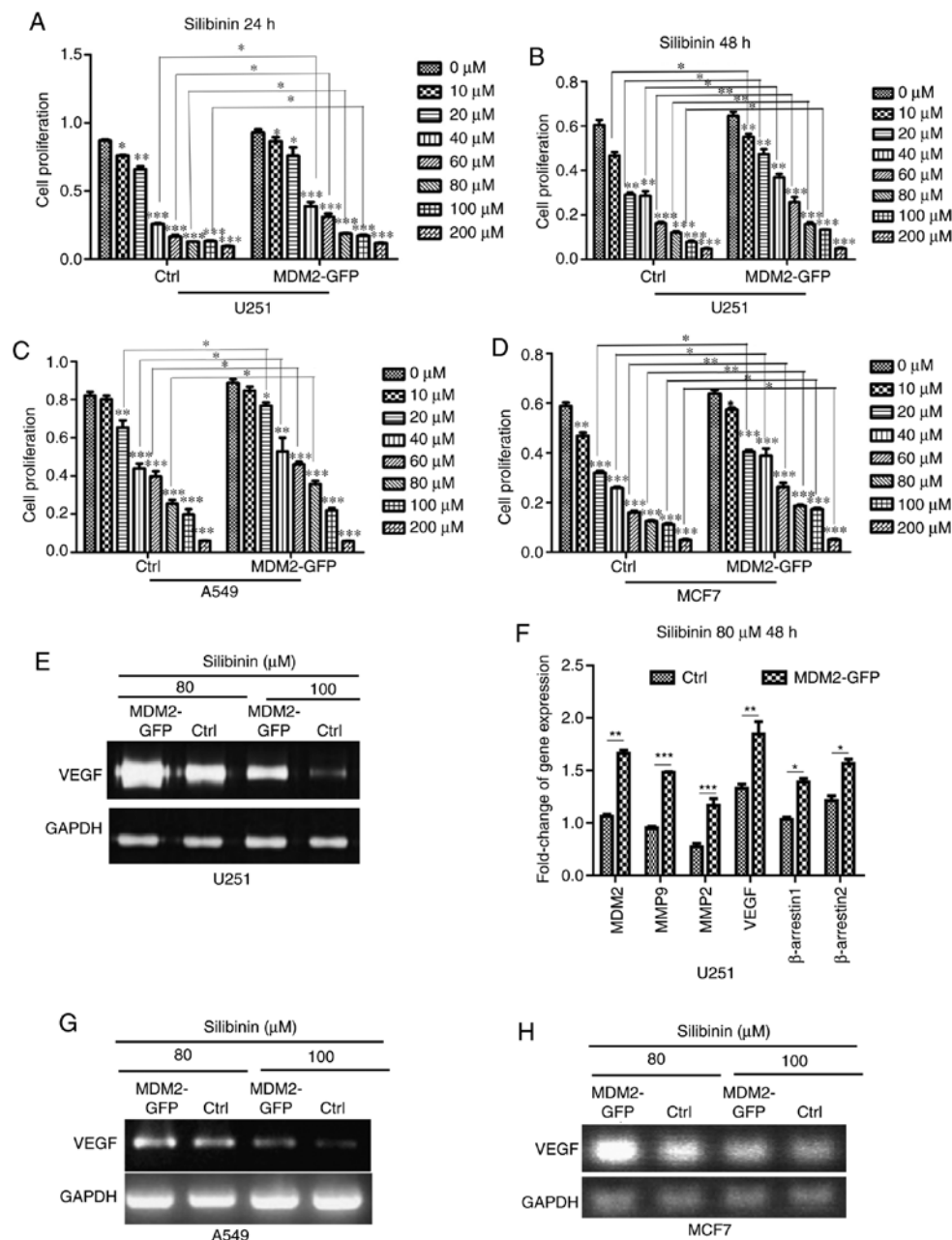
Figure 7. MDM2 overexpression prevents sensitivity to growth inhibition by silibinin in U251, A549 and MCF7 cells. (A) After cells were treated with the indicated doses of silibinin (0, 10, 20, 40, 60, 80, 100 or 200 μM), cell viabilities were determined using an MTT assay after 24 h in control U251 cells and MDM2-overexpressing U251 cells. Ctrl referred to the U251 cell line with stable overexpression of plenti-CMV-puro empty vector. (B) After cells were treated with the indicated doses of silibinin (0, 10, 20, 40, 60, 80, 100 and 200 μM), cell proliferation were determined using an MTT assay after 48 h in control U251 cells and MDM2-overexpressing U251 cells. Ctrl referred to the U251 cell line with stable overexpression of plenti-CMV-puro empty vector. (C) After cells were treated with the indicated doses of silibinin (0, 10, 20, 40, 60, 80, 100 and 200 μM), cell proliferation were determined using an MTT assay after 48 h in control A549 cells and MDM2-overexpressing A549 cells. Ctrl referred to the A549 cell line with stable overexpression of plenti-CMV-puro empty vector. (D) After cells were treated with the indicated doses of silibinin (0, 10, 20, 40, 60, 80, 100 and 200 μM), cell proliferation were determined using an MTT assay after 48 h in control MCF7 cells and MDM2-overexpressing MCF7 cells. Ctrl referred to the MCF7 cell line with stable overexpression of plenti-CMV-puro empty vector. (E) Control U251 cells and MDM2-overexpressing U251 cells were treated with the indicated doses of silibinin (80 and 100 μM) for 48 h, and total mRNA was subjected to SqRT-PCR to analyze *VEGF* expression. Ctrl referred to the U251 cell line with stable overexpression of plenti-CMV-puro empty vector. *GAPDH* served as a normalization control. (F) Total mRNA from control U251 cells and MDM2-overexpressing U251 cells was subjected to quantitative PCR to analyze the changes in *MDM2*, *β-arrestin1*, *β-arrestin2*, *MMP-2*, *MMP-9* and *VEGF* expression. Ctrl referred to the U251 cell line with stable overexpression of plenti-CMV-puro empty vector. *GAPDH* was used as a control. Quantitative analysis data are shown. (G) Control A549 cells and MDM2-overexpressing A549 cells were treated with the indicated doses of silibinin (80 and 100 μM) for 48 h, and then total mRNA was subjected to SqRT-PCR to analyze *VEGF* expression. Ctrl referred to the U251 cell line with stable overexpression of plenti-CMV-puro empty vector. *GAPDH* served as a control. (H) Control MCF7 cells and MDM2-overexpressing MCF7 cells were treated with the indicated doses of silibinin (80 and 100 μM) for 48 h, and then total mRNA was subjected to SqRT-PCR to analyze changes in *VEGF* expression. Ctrl referred to the U251 cell line with stable overexpression of plenti-CMV-puro empty vector. *GAPDH* served as a normalization control. For all quantifications, data are presented as the mean ± SD derived from three independent experiments. Statistical significance was analyzed using an unpaired Student's t-test in (F), and one-way ANOVA with Tukey's post hoc test was used to compare the indicated group and the 0 μM group within the Ctrl type, or the indicated group and the 0 μM group within the MDM2-GFP type, or two indicated groups in A-D. *P<0.05; **P<0.01; ***P<0.001 vs. 0 μM group or as indicated. β-arrestin1, subtype 1 of β-arrestin protein family; β-arrestin2, subtype 2 of β-arrestin protein family; Ctrl, control; GFP, green fluorescent protein; MDM2, MDM2 proto-oncogene, E3 ubiquitin protein ligase; SqRT-PCR, semi-quantitative reverse transcription PCR.

vemurafenib, U0126 or FR180204. Similar to the results in U251 cells, B-Raf, MEK and ERK inhibitors could all rescue a decrease in E-CAD protein expression (Fig. 4G). Furthermore, the same experiment was repeated in MCF7 cells (Fig. 4H). To summarize, MDM2 induced EMT by upregulating EMT transcription factors via activation of ERK regulated by B-Raf.

MDM2 activates B-Raf signaling through 14-3-3 and p53. As demonstrated in the aforementioned experiments, MDM2 induced EMT by upregulating EMT transcription factors through ERK. Furthermore, it was revealed that MDM2 expression was associated with the degradation of p53, thus decreasing the protein expression levels of p53 (Fig. 2E-G). Therefore, the present study aimed to explore whether the mechanism of MDM2-induced EMT depended on p53. qPCR and western blotting were used to analyze p53, E-CAD, N-CAD and VIM protein expression in control U251 cells and U251 cells overexpressing p53 together with MDM2-GFP (Figs. 5A and S2E). As shown in Fig. 5, overexpression of p53 rescued the decrease of E-CAD and inhibited the increase of N-CAD and VIM (Fig. 5A). These results indicated that the overexpression of p53 inhibited EMT induced by MDM2. In other words, MDM2-induced EMT was p53-dependent. Previous studies have reported that 14-3-3 is one of the most important p53 transcriptional targets (56-59). Notably, 14-3-3 can deactivate Raf directly and prevent its activation (24-27). The present study used western blot analysis to determine the expression levels of 14-3-3 in stable MDM2-overexpressing U251 cells and control U251 cells. As shown by the semi-quantitative analysis data, 14-3-3 expression was markedly decreased in stable MDM2-overexpressing U251 cells compared with the control group (Fig. 5B). Furthermore, as the most important downstream autophagy transcription factor of 14-3-3, transcription factor EB (TFEB) expression was decreased following MDM2 overexpression in the U251 cell line (data not shown). Previously, the relationship of 14-3-3 with B-Raf has been discussed, and it has been revealed that lower 14-3-3 expression is associated with an activated B-Raf signaling pathway (39), which was consistent with the present B-Raf signaling pathway data. Therefore, the present study aimed to verify whether MDM2 activated the B-Raf signaling pathway via 14-3-3. 14-3-3 overexpression was checked by qPCR (Fig. S2F) and MDM2, 14-3-3, E-CAD, N-CAD, VIM and p-B-Raf protein levels were analyzed by western blotting in control cells and cells stably overexpressing MDM2 together with Flag-14-3-3 (Fig. 5C). Overexpression of 14-3-3 inhibited the activation of the B-Raf signaling pathway. Notably, overexpression of 14-3-3 rescued the decrease in E-CAD and inhibited the increase in N-CAD and VIM, which meant that overexpression of 14-3-3 could prevent MDM2-induced EMT (Fig. 5C). The colony formation abilities of control cells and MDM2-overexpressing U251 cells with or without FR180204 were determined. As shown in the quantification data, MDM2 overexpression significantly increased the colony formation rate. However, this increased colony formation rate induced by MDM2 could be inhibited by treatment with an ERK inhibitor (Fig. 5D). Scratch wound assays were used to detect the migration abilities in control cells and MDM2-overexpressing U251 cells with or without FR180204 treatment. The percentage closure of the scratch was quantified at 0, 24 and 48 h after

wounding. As shown in the images of the migration and the quantification data, the percentage closure of the scratch in the MDM2 overexpression group was higher than that in the control group at 24 and 48 h post wounding (Fig. 5E). However, there was no significant difference between MDM2 U251 cells treated with FR180204 and the control group, which meant that the migration ability was inhibited by ERK inhibition in MDM2 U251 cells (Fig. 5E). To summarize, MDM2 induced EMT by activating the B-Raf signaling pathway through 14-3-3, which depended on p53.

B-Raf signaling, which is activated by MDM2, can promote glioma xenograft tumor progression. To assess whether MDM2 activated B-Raf signaling function in tumor progression, a xenograft model was established in NOD/SCID mice with U251 tumors. In agreement with the colony formation data (Fig. 5D), MDM2 expression accelerated tumor growth. By contrast, tumor growth was significantly inhibited when MDM2 was overexpressed together with 14-3-3 or when treated with an ERK inhibitor (Fig. 6A-C). These results indicated that the MDM2-activated B-Raf signaling pathway promoted clonogenicity and glioma xenograft tumor growth.

Immunohistochemical analyses also demonstrated increased N-CAD expression and decreased E-CAD expression in U251 xenografts expressing MDM2, which represented the occurrence of an EMT process (Fig. 6D). Loss of E-cadherin has been associated with accelerated tumor progression and metastasis (6,7). By contrast, EMT was inhibited in xenografts overexpressing MDM2 together with 14-3-3 or those treated with an ERK inhibitor (Fig. 6D). This demonstrated a partial EMT-like process in MDM2 tumors, which was reversed in tumors which overexpressed Flag 14-3-3 or were treated with FR180204. Collectively, these results indicated that the B-Raf signaling pathway serves as a downstream effector of MDM2, contributing to tumor progression and higher metastatic potential.

MDM2 promotes cell insensitivity to drug treatment by inducing EMT. It has been reported that EMT contributes to cancer cell resistance to chemotherapy agents (30-32). According to previous studies, numerous chemicals have little or no effect on cells that have undergone EMT in a number of cancer types, for example breast cancer cells and glioma (30-32). Therefore, the present study aimed to explore whether MDM2 could promote cell insensitivity to drug treatment by inducing EMT. Silibinin, also known as silybin, is a promising cancer treatment drug (60,61). The present study aimed to determine whether overexpression of MDM2 could affect drug sensitivities. First, stable overexpression MDM2 U251 cells and control cells were treated with indicated doses of silibinin (0, 10, 20, 40, 60, 80, 100 and 200 μM) and cell viability was determined using an MTT assay after 24 h. As shown in the quantification data, control cells were more sensitive to 40, 60, 80 and 100 μM silibinin treatment than MDM2-U251 cells at 24 h (Fig. 7A). Subsequently, an MTT assay was used again after 48 h in these two cell lines. Similar to the data from 24 h, control cells were more sensitive to silibinin treatment than MDM2-U251 cells at 48 h (Fig. 7B). This suggested that MDM2 promoted cell insensitivity to silibinin by inducing EMT in the U251 glioma cell line. Furthermore,
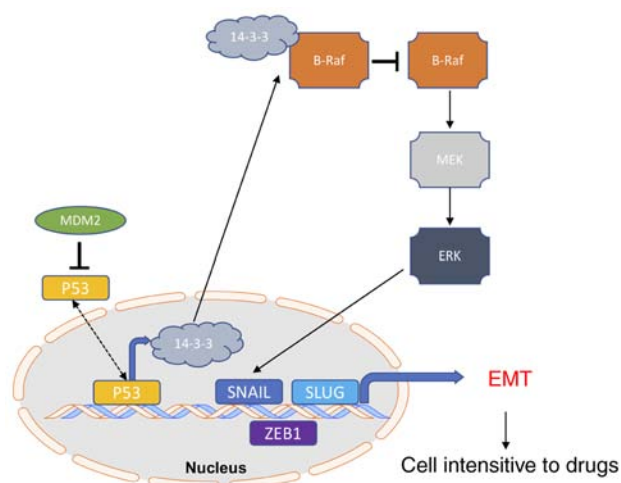
Figure 8. Model of MDM2-mediated B-Raf signaling pathway activation through 14-3-3 inducing p53-dependent EMT progression and altering cell sensitivities to cancer drugs. MDM2 may regulate the transcriptional activity of the EMT transcription factors Snail, Slug and ZEB1 through B-Raf and p53-dependent mechanisms, resulting in decreased net production of 14-3-3, which can activate B-Raf. Activation of B-Raf induces the B-Raf signaling pathway. Subsequently, ERK1/2 activates the EMT transcription factors Snail, Slug and ZEB1, which promotes EMT progression. EMT progression induces cells to have different sensitivities to drugs in cell lines and tumors. 14-3-3, tyrosine 3-monooxygenase activation protein ε; EMT, epithelial-to-mesenchymal transition; MDM2, MDM2 proto-oncogene, E3 ubiquitin protein ligase; Slug, Snail family transcriptional repressor 2; Snail, Snail family transcriptional repressor 1; ZEB1, zinc finger E-box binding homeobox 1.

this was verified in an A549 cell model. As shown in the quantification data, control cells were more sensitive to 20, 40, 60 and 80 μM silibinin treatment than MDM2-GFP cells at 48 h in A549 cell model (Fig. 7C). Control cells were more sensitive to 20-200 μM silibinin treatment than MDM2-GFP cells in an MCF7 cell model (Fig. 7D). According to previous literature reports, silibinin inhibits the relevant pathways for angiogenesis and decreases the expression of VEGF and other related genes (35,36). Therefore, total mRNA was subjected to SqRT-PCR to analyze changes in VEGF expression in U251 cells (Fig. 7E). *MDM2*, *β-arrestin1*, *β-arrestin2*, *MMP-2*, *MMP-9* and *VEGF* expression was analyzed by qPCR (Fig. 7F). According to SqRT-PCR and qPCR, MDM2 overexpression rescued the decreased expression of *β-arrestin1*, *β-arrestin2*, *MMP-2*, *MMP-9* and *VEGF*, which are downstream genes of silibinin. Subsequently, the changes in *VEGF* expression were also verified by SqRT-PCR in A549 and MCF7 cell models (Fig. 7G and H). Therefore, MDM2 induced EMT by upregulating EMT transcription factors via activation of the B-Raf signaling pathway through 14-3-3, and this depended on p53. Subsequently, the EMT induced by MDM2 could promote cell insensitivity to drug treatment (Fig. 8).

Discussion

The present study utilized SqRT-PCR, qPCR, GSEA, scratch wound assays and western blotting, and revealed that MDM2 overexpression increased migration and induced EMT in three cell models. EMT serves a crucial role in tumor development (6). The present data regarding MDM2 provide a

novel direction for tumor research. MDM2 is involved in the invasion and metastasis of tumor cells (62,63). MDM2 overexpression can increase the expression of EMT transcranial factors, such as Snail, Slug and ZEB1; however, these factors are not only associated with EMT (62-64). MDM2 can take part in other physiological mechanisms by regulating Snail, Slug and ZEB1 (64,65). Previous studies have reported that Raf/MEK/ERK signaling serves a role in the EMT process (39,66). The present study explored the mechanism of Raf/MEK/ERK signaling involved in and affecting EMT. Using scratch wound assays, colony formation assays, western blotting and *in vivo* experiments, it was demonstrated that B-Raf-MEK-ERK signaling serves as a downstream effector of MDM2.

The present study also demonstrated that the B-Raf-MEK-ERK signaling pathway was activated, while the mTOR signaling pathway and ERK downstream RSK pathway were not involved in the EMT process induced by MDM2. The Raf/MEK/ERK signaling pathway is associated with other important physiological mechanisms, such as autophagy and lysosome biogenesis (67,68). However, to the best of our knowledge, whether MDM2 may also take part in autophagy and lysosome biogenesis through the Raf/MEK/ERK signaling pathway is unclear. According to the present *in vitro* and *in vivo* experiments, MDM2 activated the B-Raf signaling pathway, and induced EMT and tumor progression through 14-3-3. The present data highlighted an important research direction for future cancer research.

The most important finding of the present study was that it revealed the relationship between MDM2 and 14-3-3. 14-3-3 is involved in regulating multiple cellular processes. There is growing evidence that 14-3-3 serves an important role in human cancer and neurological diseases (17-23). Therefore, it was hypothesized that MDM2 may also participate in these important processes through 14-3-3 regulation. Importantly, 14-3-3 is an important regulator of the autophagy transcription factor TFEB (69-71). The preliminary experimental data has indicated that MDM2 decreased TFEB expression in the U251 cell line (data not shown). Whether MDM2 participates in autophagy management through 14-3-3 regulation of TFEB remains unclear.

A significant amount of evidence has indicated that the actions of MDM2 and p53 are closely related. MDM2 inhibits p53 by ubiquitinating and degrading p53 (2,3). p53 is a widely studied factor associated with apoptosis and other related mechanisms (72,73). Therefore, MDM2 may be used in clinical therapy of the numerous diseases in which p53 is involved. EMT has been reported to contribute to cancer cells becoming resistant to chemotherapy agents (74,75). The present study indicated that MDM2 promoted cell insensitivity to silibinin treatment by inducing EMT in three cell models. However, the mechanism of EMT-induced drug sensitivity is still unclear (76). The present study also demonstrated possible directions for future research investigating the association between MDM2 and drug resistance in clinical settings.

Although the present study revealed a novel mechanism of the MDM2-induced EMT process and indicated that MDM2 promote cell insensitivity to silibinin treatment, whether MDM2 influences other biological mechanisms through the BRAF signaling pathway or not is unclear. The preliminary

experimental data has indicated that MDM2 decreased TFEB expression (data not shown). It is unknown whether MDM2 can interfere with autophagy and lysosomal signals through TFEB, which is an important autophagy-lysosomal transcription factor. The current hypothesis that autophagy inhibition may promote tumor inhibition and chemosensitivity is largely based on studies of anti-tumor effects of the lysosomotropic agent or its derivatives in combination cancer chemotherapy (39,66). In addition, previous studies have uncovered a unappreciated role for TFEB-mediated autophagy-lysosomal activation in suppressing TGF-β signaling, and revealed that TFEB blockade enhances TGF-β secretion and signaling (67,68). These studies have demonstrated an association between B-Raf, TFEB, TGF-β-EMT, autophagy and tumor resistance. However, the relationship between MDM2, autophagy-lysosome, TFEB and tumor chemosensitivity is unknown. Therefore, it is important to understand the association between MDM2 and autophagy and chemosensitivity in future studies. At least, the present study provided theoretical support to explore these mechanisms.

In conclusion, MDM2 induced EMT by upregulating EMT transcription factors via activation of the B-Raf signaling pathway through 14-3-3, and this depended on p53 (Fig. 8). This finding will become a crucial paradigm for research in cancer therapy and can provide novel research directions for future biological and clinical research.

Acknowledgements

Availability of data and materials

The RNA-Seq datasets generated and/or analyzed during the current study are available in the Gene Expression Omnibus repository (https://www.ncbi.nlm.nih.gov/geo/query/acc.cgi?acc=GSE165030). The GSEA and other datasets used and/or analyzed during the current study are available from the corresponding author on reasonable request.

Authors' contributions

LT and JF conceptualized and designed the research. MO, XX, YC, YL and LL performed the experiments. YL and JF contributed reagents and collected clinical samples. CQ, LZ and WS analyzed the data. MO and CQ wrote and revised the manuscript. LT, JF and MO confirm the authenticity of all the raw data. All authors read and approved the final manuscript and agree to be accountable for all aspects of the research in ensuring that the accuracy or integrity of any part of the work are appropriately investigated and resolved.

Ethics approval and consent to participate

All experiments were performed in accordance with the guidelines and complied with ethical standards. All clinical tumor samples were obtained according to clinical guidelines and in compliance with ethical standards (approval no. Y2019045; Southwest Medical University Ethics Committee, Luzhou, China). The informed consent document was signed by each patient to agree to the use of their samples in scientific research. All animal studies were performed in accordance with the guidelines. The research was reviewed and approved by ethical committee before conduction (approval no. 201903-34; Southwest Medical University Ethics Committee, Luzhou, China).

Patient consent for publication

Not applicable.

Competing interests

The authors declare that they have no competing interests.

References

1. Fakharzadeh SS, Trusko SP and George DL: Tumorigenic potential associated with enhanced expression of a gene that is amplified in a mouse tumor cell line. EMBO J 10: 1565-1569, 1991.
2. Xia YZ, Yang L, Xue GM, Zhang C, Guo C, Yang YW, Li SS, Zhang LY, Guo QL and Kong LY: Combining GRP78 suppression and MK2206-induced Akt inhibition decreases doxorubicin-induced P-glycoprotein expression and mitigates chemoresistance in human osteosarcoma. Oncotarget 7: 56371-56382, 2016.
3. Haupt Y, Maya R, Kazaz A and Oren M: Mdm2 promotes the rapid degradation of p53. Nature 387: 296-299, 1997.
4. Momand J, Zambetti GP, Olson DC, George D and Levine AJ: The mdm-2 oncogene product forms a complex with the p53 protein and inhibits p53-mediated transactivation. Cell 69: 1237-1245, 1992.
5. Jung CR, Lim JH, Choi Y, Kim DG, Kang KJ, Noh SM and Im DS: Enigma negatively regulates p53 through MDM2 and promotes tumor cell survival in mice. J Clin Invest 120: 4493-4506, 2010.
6. Thiery JP: Epithelial-mesenchymal transitions in cancer onset and progression. Bull Acad Natl Med 193: 1969-1979, 2009 (In French).
7. Iwakuma T and Agarwal N: MDM2 binding protein, a novel metastasis suppressor. Cancer Metastasis Rev 31: 633-640, 2012.
8. Wang SP, Wang WL, Chang YL, Wu CT, Chao YC, Kao SH, Yuan A, Lin CW, Yang SC, Chan WK, et al: p53 controls cancer cell invasion by inducing the MDM2-mediated degradation of Slug. Nat Cell Biol 11: 694-704, 2009.
9. Osborne JK, Zaganjor E and Cobb MH: Signal control through Raf: In sickness and in health. Cell Res 22: 14-22, 2012.
10. Stephen AG, Esposito D, Bagni RK and McCormick F: Dragging ras back in the ring. Cancer Cell 25: 272-281, 2014.
11. Min L, He B and Hui L: Mitogen-activated protein kinases in hepatocellular carcinoma development. Semin Cancer Biol 21: 10-20, 2011.
12. Tzivion G, Gupta VS, Kaplun L and Balan V: 14-3-3 proteins as potential oncogenes. Semin Cancer Biol 16: 203-213, 2006.
13. Zhang J and Zhou Y: 14-3-3 Proteins in glutamatergic synapses. Neural Plast 2018: 8407609, 2018.
14. Vergroesen PP, Kingma I, Emanuel KS, Hoogendoorn RJ, Welting TJ, van Royen BJ, van Dieën JH and Smit TH: Mechanics and biology in intervertebral disc degeneration: A vicious circle. Osteoarthritis Cartilage 23: 1057-1070, 2015.

15. Stevers LM, Sijbesma E, Botta M, MacKintosh C, Obsil T, Landrieu I, Cau Y, Wilson AJ, Karawajczyk A, Eickhoff J, *et al*: Modulators of 14-3-3 protein-protein interactions. J Med Chem 61: 3755-3778, 2018.
16. Park E, Rawson S, Li K, Kim BW, Ficarro SB, Pino GG, Sharif H, Marto JA, Jeon H and Eck MJ: Architecture of autoinhibited and active BRAF-MEK1-14-3-3 complexes. Nature 575: 545-550, 2019.
17. Aitken A: 14-3-3 proteins: A historic overview. Semin Cancer Biol 16: 162-172, 2006.
18. Li X, Wang QJ, Pan N, Lee S, Zhao Y, Chait BT and Yue Z: Phosphorylation-dependent 14-3-3 binding to LRRK2 is impaired by common mutations of familial Parkinson's disease. PLoS One 6: e17153, 2011.
19. Nichols RJ, Dzamko N, Morrice NA, Campbell DG, Deak M, Ordureau A, Macartney T, Tong Y, Shen J, Prescott AR and Alessi DR: 14-3-3 binding to LRRK2 is disrupted by multiple Parkinson's disease-associated mutations and regulates cytoplasmic localization. Biochem J 430: 393-404, 2010.
20. Kilani RT, Maksymowych WP, Aitken A, Boire G, St-Pierre Y, Li Y and Ghahary A: Detection of high levels of 2 specific isoforms of 14-3-3 proteins in synovial fluid from patients with joint inflammation. J Rheumatol 34: 1650-1657, 2007.
21. Neal CL and Yu D: 14-3-3ζ as a prognostic marker and therapeutic target for cancer. Expert Opin Ther Targets 14: 1343-1354, 2010.
22. Lamba S, Ravichandran V and Major EO: Glial cell type-specific subcellular localization of 14-3-3 zeta: An implication for JCV tropism. Glia 57: 971-977, 2009.
23. Kelly MN, Johnston DA, Peel BA, Morgan TW, Palmer GE and Sturtevant JE: Bmh1p (14-3-3) mediates pathways associated with virulence in Candida albicans. Microbiology (Reading) 155: 1536-1546, 2009.
24. Halbach T, Scheer N and Werr W: Transcriptional activation by the PHD finger is inhibited through an adjacent leucine zipper that binds 14-3-3 proteins. Nucleic Acids Res 28: 3542-3550, 2000.
25. Ritt DA, Monson DM, Specht SI and Morrison DK: Impact of feedback phosphorylation and Raf heterodimerization on normal and mutant B-Raf signaling. Mol Cell Biol 30: 806-819, 2010.
26. Tzivion G and Avruch J: 14-3-3 proteins: Active cofactors in cellular regulation by serine/threonine phosphorylation. J Biol Chem 277: 3061-3064, 2002.
27. Tzivion G, Luo Z and Avruch J: A dimeric 14-3-3 protein is an essential cofactor for Raf kinase activity. Nature 394: 88-92, 1998.
28. Liau NPD, Wendorff TJ, Quinn JG, Steffek M, Phung W, Liu P, Tang J, Irudayanathan FJ, Izadi S, Shaw AS, *et al*: Negative regulation of RAF kinase activity by ATP is overcome by 14-3-3-induced dimerization. Nat Struct Mol Biol 27: 134-141, 2020.
29. Kondo Y, Ognjenović J, Banerjee S, Karandur D, Merk A, Kulhanek K, Wong K, Roose JP, Subramaniam S and Kuriyan J: Cryo-EM structure of a dimeric B-Raf:14-3-3 complex reveals asymmetry in the active sites of B-Raf kinases. Science 366: 109-115, 2019.
30. Ahmed N, Abubaker K, Findlay J and Quinn M: Epithelial mesenchymal transition and cancer stem cell-like phenotypes facilitate chemoresistance in recurrent ovarian cancer. Curr Cancer Drug Targets 10: 268-278, 2010.
31. Wang TH, Wang HS and Soong YK: Paclitaxel-induced cell death: Where the cell cycle and apoptosis come together. Cancer 88: 2619-2628, 2000.
32. Yang Q, Huang J, Wu Q, Cai Y, Zhu L, Lu X, Chen S, Chen C and Wang Z: Acquisition of epithelial-mesenchymal transition is associated with Skp2 expression in paclitaxel-resistant breast cancer cells. Br J Cancer 110: 1958-1967, 2014.
33. Zhang P, Liu H, Xia F, Zhang QW, Zhang YY, Zhao Q, Chao ZH, Jiang ZW and Jiang CC: Epithelial-mesenchymal transition is necessary for acquired resistance to cisplatin and increases the metastatic potential of nasopharyngeal carcinoma cells. Int J Mol Med 33: 151-159, 2014.
34. Gu MF, Liu LZ, He LJ, Yuan WX, Zhang R, Luo GY, Xu GL, Zhang HM, Yan CX and Li JJ: Sequential chemoradiotherapy with gemcitabine and cisplatin for locoregionally advanced nasopharyngeal carcinoma. Int J Cancer 132: 215-223, 2013.
35. Li QQ, Xu JD, Wang WJ, Cao XX, Chen Q, Tang F, Chen ZQ, Liu XP and Xu ZD: Twist1-mediated adriamycin-induced epithelial-mesenchymal transition relates to multidrug resistance and invasive potential in breast cancer cells. Clin Cancer Res 15: 2657-2665, 2009.
36. McConkey DJ, Choi W, Marquis L, Martin F, Williams MB, Shah J, Svatek R, Das A, Adam L, Kamat A, *et al*: Role of epithelial-to-mesenchymal transition (EMT) in drug sensitivity and metastasis in bladder cancer. Cancer Metastasis Rev 28: 335-344, 2009.
37. Li L, Feng J, Chen Y, Li S, Ou M, Sun W and Tang L: Estradiol shows anti-skin cancer activities through decreasing MDM2 expression. Oncotarget 8: 8459-8474, 2017.
38. Li S, Ma L, Ou M, Feng J, Liao Y, Wang G and Tang L: A novel inducible lentiviral system for multi-gene expression with human HSP70 promoter and tetracycline-induced promoter. Appl Microbiol Biotechnol 101: 3689-3702, 2017.
39. Li S, Song Y, Quach C, Guo H, Jang GB, Maazi H, Zhao S, Sands NA, Liu Q, In GK, *et al*: Transcriptional regulation of autophagy-lysosomal function in BRAF-driven melanoma progression and chemoresistance. Nat Commun 10: 1693, 2019.
40. Livak KJ and Schmittgen TD: Analysis of relative gene expression data using real-time quantitative PCR and the 2(-Delta Delta C(T)) method. Methods 25: 402-408, 2001.
41. Weselling P and Capper D: WHO 2016 classification of gliomas. Neuropathol Appl Neurobiol 44: 139-150, 2018.
42. Lu X, Yan C, Huang Y, Shi D, Fu Z, Qiu J and Yin Y: Mouse double minute 2 (MDM2) upregulates Snail expression and induces epithelial-to-mesenchymal transition in breast cancer cells in vitro and in vivo. Oncotarget 7: 37177-37191, 2016.
43. Galvan JA, Zlobec I, Wartenberg M, Lugli A, Gloor B, Perren A and Karamitopoulou E: Expression of E-cadherin repressors SNAIL, ZEB1 and ZEB2 by tumour and stromal cells influences tumour-budding phenotype and suggests heterogeneity of stromal cells in pancreatic cancer. Br J Cancer 112: 1944-1950, 2015.
44. Schulte J, Weidig M, Balzer P, Richter P, Franz M, Junker K, Gajda M, Friedrich K, Wunderlich H, Östman A, *et al*: Expression of the E-cadherin repressors Snail, Slug and Zeb1 in urothelial carcinoma of the urinary bladder: Relation to stromal fibroblast activation and invasive behaviour of carcinoma cells. Histochem Cell Biol 138: 847-860, 2012.
45. Weichhart T: mTOR as regulator of lifespan, aging, and cellular senescence: A Mini-review. Gerontology 64: 127-134, 2018.
46. Bertacchini J, Heidari N, Mediani L, Capitani S, Shahjahani M, Ahmadzadeh A and Saki N: Targeting PI3K/AKT/mTOR network for treatment of leukemia. Cell Mol Life Sci 72: 2337-2347, 2015.
47. Hermida MA, Dinesh Kumar J and Leslie NR: GSK3 and its interactions with the PI3K/AKT/mTOR signalling network. Adv Biol Regul 65: 5-15, 2017.
48. Bollag G, Hirth P, Tsai J, Zhang J, Ibrahim PN, Cho H, Spevak W, Zhang C, Zhang Y, Habets G, *et al*: Clinical efficacy of a RAF inhibitor needs broad target blockade in BRAF-mutant melanoma. Nature 467: 596-599, 2010.
49. Garber K: Cancer research. Melanoma drug vindicates targeted approach. Science 326: 1619, 2009.
50. DeSilva DR, Jones EA, Favata MF, Jaffee BD, Magolda RL, Trzaskos JM and Scherle PA: Inhibition of mitogen-activated protein kinase kinase blocks T cell proliferation but does not induce or prevent anergy. J Immunol 160: 4175-4181, 1998.
51. Favata MF, Horiuchi KY, Manos EJ, Daulerio AJ, Stradley DA, Feeser WS, Van Dyk DE, Pitts WJ, Earl RA, Hobbs F, *et al*: Identification of a novel inhibitor of mitogen-activated protein kinase kinase. J Biol Chem 273: 18623-18632, 1998.
52. Ohori M, Takeuchi M, Maruki R, Nakajima H and Miyake H: FR180204, a novel and selective inhibitor of extracellular signal-regulated kinase, ameliorates collagen-induced arthritis in mice. Naunyn Schmiedebergs Arch Pharmacol 374: 311-316, 2007.
53. Alexaki VI, Javelaud D, Van Kempen LC, Mohammad KS, Dennler S, Luciani F, Hoek KS, Juàrez P, Goydos JS, Fournier PJ, *et al*: GLI2-mediated melanoma invasion and metastasis. J Natl Cancer Inst 102: 1148-1159, 2010.
54. Smith JA, Maloney DJ, Hecht SM and Lannigan DA: Structural basis for the activity of the RSK-specific inhibitor, SL0101. Bioorg Med Chem 15: 5018-5034, 2007.
55. Smith JA, Maloney DJ, Clark DE, Xu Y, Hecht SM and Lannigan DA: Influence of rhamnose substituents on the potency of SL0101, an inhibitor of the Ser/Thr kinase, RSK. Bioorg Med Chem 14: 6034-6042, 2006.
56. Hu W, Feng Z and Levine AJ: The regulation of multiple p53 stress responses is mediated through MDM2. Genes Cancer 3: 199-208, 2012.
57. Chen DY, Dai DF, Hua Y and Qi WQ: p53 suppresses 14-3-3γ by stimulating proteasome-mediated 14-3-3γ protein degradation. Int J Oncol 46: 818-824, 2015.

58. Radhakrishnan VM, Putnam CW, Qi W and Martinez JD: P53 suppresses expression of the 14-3-3γ oncogene. BMC Cancer 11: 378, 2011.
59. Zhang Y, Dube C, Gibert M Jr, Cruickshanks N, Wang B, Coughlan M, Yang Y, Setiady I, Deveau C, Saoud K, et al: The p53 pathway in glioblastoma. Cancers 10: 297, 2018.
60. Singh RP and Agarwal R: Cosmeceuticals and silibinin. Clin Dermatol 27: 479-484, 2009.
61. Cheung CW, Gibbons N, Johnson DW and Nicol DL: Silibinin-a promising new treatment for cancer. Anticancer Agents Med Chem 10: 186-195, 2010.
62. Hauck PM, Wolf ER, Olivos DJ III, Batuello CN, McElyea KC, McAtarsney CP, Cournoyer RM, Sandusky GE and Mayo LD: Early-stage metastasis requires Mdm2 and Not p53 gain of function. Mol Cancer Res 15: 1598-1607, 2017.
63. Chen Y, Wang DD, Wu YP, Su D, Zhou TY, Gai RH, Fu YY, Zheng L, He QJ, Zhu H and Yang B: MDM2 promotes epithelial-mesenchymal transition and metastasis of ovarian cancer SKOV3 cells. Br J Cancer 117: 1192-1201, 2017.
64. Her NG, Oh JW, Oh YJ, Han S, Cho HJ, Lee Y, Ryu GH and Nam DH: Potent effect of the MDM2 inhibitor AMG232 on suppression of glioblastoma stem cells. Cell Death Dis 9: 792, 2018.
65. Jung CH, Kim J, Park JK, Hwang SG, Moon SK, Kim WJ and Um HD: Mdm2 increases cellular invasiveness by binding to and stabilizing the Slug mRNA. Cancer Lett 335: 270-277, 2013.
66. Lionarons DA, Hancock DC, Rana S, East P, Moore C, Murillo MM, Carvalho J, Spencer-Dene B, Herbert E, Stamp G, et al: RAC1^{P29S} induces a mesenchymal phenotypic switch via serum response factor to promote melanoma development and therapy resistance. Cancer Cell 36: 68-83.e9, 2019.
67. Li S, Song Y, Quach C, Nemecio D and Liang C: Revisiting the role of autophagy in melanoma. Autophagy 15: 1843-1844, 2019.
68. Klionsky DJ, Abdelmohsen K, Abe A, Abedin MJ, Abeliovich H, Acevedo Arozena A, Adachi H, Adams CM, Adams PD, Adeli K, et al: Guidelines for the use and interpretation of assays for monitoring autophagy (3rd edition). Autophagy 12: 1-222, 2016.
69. Xu Y, Ren J, He X, Chen H, Wei T and Feng W: YWHA/14-3-3 proteins recognize phosphorylated TFEB by a noncanonical mode for controlling TFEB cytoplasmic localization. Autophagy 15: 1017-1030, 2019.
70. Zhitomirsky B, Yunaev A, Kreiserman R, Kaplan A, Stark M and Assaraf YG: Lysosomotropic drugs activate TFEB via lysosomal membrane fluidization and consequent inhibition of mTORC1 activity. Cell Death Dis 9: 1191, 2018.
71. Nezich CL, Wang C, Fogel AI and Youle RJ: MiT/TFE transcription factors are activated during mitophagy downstream of Parkin and Atg5. J Cell Biol 210: 435-450, 2015.
72. Hafner A, Bulyk ML, Jambhekar A and Lahav G: The multiple mechanisms that regulate p53 activity and cell fate. Nat Rev Mol Cell Biol 20: 199-210, 2019.
73. Robin M, Issa AR, Santos CC, Napoletano F, Petitgas C, Chatelain G, Ruby M, Walter L, Birman S, Domingos PM, et al: Drosophila p53 integrates the antagonism between autophagy and apoptosis in response to stress. Autophagy 15: 771-784, 2019.
74. Shibue T and Weinberg RA: EMT, CSCs, and drug resistance: The mechanistic link and clinical implications. Nat Rev Clin Oncol 14: 611-629, 2017.
75. Xu X, Zhang L, He X, Zhang P, Sun C, Xu X, Lu Y and Li F: TGF-β plays a vital role in triple-negative breast cancer (TNBC) drug-resistance through regulating stemness, EMT and apoptosis. Biochem Biophys Res Commun 502: 160-165, 2018.
76. Hata AN, Rowley S, Archibald HL, Gomez-Caraballo M, Siddiqui FM, Ji F, Jung J, Light M, Lee JS, Debussche L, et al: Synergistic activity and heterogeneous acquired resistance of combined MDM2 and MEK inhibition in KRAS mutant cancers. Oncogene 36: 6581-6591, 2017.